HEFAT2014
10th International Conference on Heat Transfer, Fluid Mechanics and Thermodynamics

14 – 16 July 2014

Orlando, Florida

BUBBLE DEFORMATION IN NUCLEATE BOILING

C.W.M. van der Geld
Department of Mechanical Engineering,
Eindhoven University of Technology,
P.O. Box 513, 5600 MB Eindhoven,
The Netherlands,
E-mail: c.w.m.v.d.geld@tue.nl

ABSTRACT

Various aspects of boiling bubble deformation and oscillation have been examined or re-examined with an Euler-Lagrange approach. Anisotropic bubble deformation is easily converted into the acoustically powerful isotropic breathing mode. The structure of the added mass matrix involved explains this conversion. With a perturbation analysis, resonance cases in which this conversion is amplified or in which several different bubble sizes at a time are excited have been identified. The effects of finite disturbance amplitude and the proximity of the wall on oscillation frequency have been quantified.

Experimental validation is reported of frequency reduction by the presence of the wall or by fixation of the bubble foot to a wall.

NOMENCLATURE

A_b	[m^2]	area of bubble surface
b_m	[m]	coefficients in expansion for R
b_k	[-]	time-dependent generalized coordinate which also serve as spectral coefficients
F	[-]	ratio of frequencies squared, ω_L^2/ω_{RP}^2
g	[-]	R_0/h
h	[m]	distance of the center to the wall
h_L	[J/kg]	specific enthalpy of the liquid
h_V	[J/kg]	specific enthalpy of the vapor
k		resonance indicator: $\{p_L R_0/\sigma\}^2 / \{ 16/\gamma - 2 + 2/(3\gamma) \}$
m		exponent, to be fitted.
p_o	[Pa]	initial pressure inside the bubble
p_b	[Pa]	pressure inside the bubble
p_L	[Pa]	pressure in the liquid
p_∞	[Pa]	pressure in the liquid far away from the bubble
P_k		zero order Legendre polynomial; $P_0=1$; $P_1(x) = x$, …
Psl	[-]	ratio of system pressure to inertia pressure, $p_\infty / (\rho_L U_0^2)$
Q		generalized force
r	[m]	radial coordinate in polar coordinate system,
R_0	[m]	initial amplitude of the isotropic breathing mode: $b_1(t=0)$
Re	[-]	Reynolds number, $U_0 R_0 \rho_L / \mu_L$
T	[s]	period of oscillation
T_L		kinetic energy in the fluid outside a bubble
T_w	[^{o}C]	temperature of the wall
T_{sat}	[^{o}C]	saturation temperature
U	[m/s]	velocity component normal to the wall
v	[m/s]	velocity
V_b	[m^3]	bubble volume
We	[-]	Weber number, $U_0^2 \rho_L R_0 / \sigma$

Special characters

$\dot{b}_3$		the third generalized velocity component
β	[–]	initial dimensionless amplitude of the anisotropic deformation mode: $b_3(t=0)/R_0$
Δh	[J/kg]	enthalpy of evaporation
γ		ratio of specific heats, c_p/c_v
θ	[radian]	polar angle in polar coordinate system
λ		ratio of observed radian frequency, ω_3, to ω_L: ω_3 / ω_L
μ	[Ns/m^2]	dynamic viscosity
ρ_L	[kg/m^3]	mass density of the liquid
σ	[N/m]	surface tension coefficient between liquid and vapor
τ_{osc}	[-]	dimensionless oscillation time, $\sqrt{(\rho_L R_0^3 / \sigma)}$
ψ		$(k-1)(25-3\gamma)+24$
ψ_{ij}		added mass coefficients
ω	[Hz]	radian frequency. $\omega_L^2 = 12\,\sigma/(\rho_L R_0^3)$; $\omega_{RP}^2 = 3\,\gamma p_{l}/(\rho_L R_0^2) + (3\gamma-1)2\sigma/(\rho_L R_0^3)$

Subscripts

b	bubble
I	interface
L	liquid
sat	saturation
v	vapor, bubble content
w	wall

INTRODUCTION

Nucleate boiling is one of the most efficient modes of heat transfer, yet many aspects of nucleate boiling are not well understood even today. Important aspects of nucleate flow boiling currently under research concern

- the effect of the angle of inclination and approaching flow on bubble deformation and detachment

- the effect of sound on bubble nucleation, growth and detachment
- interaction of neighboring bubble nucleation sites, via convection and via bubble-bubble interaction.

Also in the last example bubble deformation has been found to play an important role. The net heat transfer coefficient depends strongly on all these phenomena. The predictive capacity of phenomenological, or mechanistic, heat transfer and pressure drop models suffers nevertheless from a lack of knowledge of these phenomena. This study therefore deals with deformation and oscillation of boiling bubbles.

Bubble or drop oscillation is a rich topic with many interesting physical phenomena playing a role, with diverse applications and with many studies reported in the open literature. A bubble or drop is a nice example of a spring-mass system that may oscillate for long times if viscosity is small. The inertial mass represents kinetic energy that is converted into potential energy provided mainly by surface tension at the vapor-liquid interface; the pressure contribution of the bubble content is usually small. The oscillatory behavior of such a system has been studied for centuries. The various modes of deformation of free drops and bubbles were already predicted in the 19th century, see Lamb [1]. Since that time, analytical studies mainly concerned linear approximations of deformation [2, 3, 4, 5]. A nonlinear theory for air bubbles was for example given by Longuet-Higgins [6], who performed a perturbation analysis of three sets of parameters (velocity potential, interface, pressure) simultaneously. The last decades many numerical studies were devoted to bubble and drop oscillation [7, 8, 9], as well as some experimental ones [10, 11]. In recent years, analytical studies of linear deformation of constrained bubbles were carried out [12, 13]. The solution method utilizes a set of orthonormal basis functions different from the Legendre polynomials used by Lamb in order to satisfy the constraints. The stable shape of a bubble attached to a circular hole in a wall, with gravity acting perpendicular to the wall but without motion, was analytically predicted by Chesters in the 70's of the last century [14]. Other stable drop shapes in the absence of motion were merely predicted numerically. Dimensionless numbers were used to characterize the shapes and generalize the findings.

Many numerical studies concerned solutions of the Rayleigh-Plesset equation [8]. In particular when a bubble collapses, peculiar physical phenomena may occur which increase the temperature of the bubble content. Pioneering work on these phenomena was carried out by Brenner *et al.* [15]. Sound generation by bubble deformation requires [16] terms with v_I /c in the Rayleigh-Plesset equation, v_I being the interface velocity and c that of sound. The topic of bubble deformation is that rich that bubble collapse will not be covered by the present paper. Sound generation by bubble oscillations will be computed neither, but knowledge about sound generation by bubbles is utilized to focus attention to isotropic bubble deformation in the context of sound production. It is well known [17, 18, 19, 20] that if bubbles are capable of responding as an acoustic monopole, an acoustic activity of considerable magnitude may develop [21]. Acoustic monopoles correspond to isotropic bubble deformation, the so-called breathing mode [22]. Ambient noise in the ocean, for example, is believed to be partly caused by oscillating bubbles. Bubbles in the ocean may result from wave breaking, splashes, rain and biological activity. The onset of wave breaking is marked by an increase of noise at frequencies exceeding a few hundred Hz. Bubbles have been observed to penetrate several meters under the ocean surface [17, 18, 21]. Bubbles in the ocean respond to the pressure fluctuations by deforming. It is therefore interesting to explore which mechanisms can transform anisotropic bubble deformation into the powerful breathing mode.

Heat transfer plays a natural role in boiling bubble growth. Each time a hot liquid patch comes in the vicinity of a heated wall with a natural or artificial cavity, nucleation might commence. The pressure in the cavity needs to exceed the pressure required to expand the vapor-liquid interface and the superheat in the hot liquid patch need to be sufficient to cause boiling bubble growth. If the superheat is insufficient, the bubble will collapse without reaching full growth with detachment from the wall. At each instant of time, the bubble shape needs to be stable in the sense that if all fluid dynamic forces are taken into account the sum of all forces must satisfy Newton's second law. This shows that force balances alone can never predict bubble detachment.

Boiling bubble growth is often proclaimed to be stochastic. Of course, the hot patches arriving near the nucleation site are turbulent patches, usually, and turbulence is inherently stochastic. But the time of flight of such a patch is negligible as compared to the growth time of a bubble, so heat transfer and fluid motion near the bubble are during its growth *not* essentially stochastic. If we were able to measure the instantaneous temperature field near the nucleation site, this would suffice as an initial condition for the heat transfer to the expanding interface. Of course, also nucleation has stochastic features in the sense that activation of a site depends on inert gas remnants near the site and the heating and system pressure history. Not always the same site is activated, let alone the possibility that a natural cavity is changing shape by pollution, oxide layer or is deactivated by dynamic air removal. Despite all these agencies, the reproducibility of bubble growth curves can be very high even in convective boiling. One must take care to consider only bubbles originating from the same site. Stochastic modeling is therefore not studied in the present paper.

Isotropic oscillations with heat transfer free bubble were studied by Prosperetti and coworkers [23] and by Nigmatulin [16] and Gumerov [24, 25]. The boundary condition for heat transfer at the liquid-vapor interface is a Stefan condition for a moving interface with mass transfer across the interface and with motion in an essentially 3D (spherical) flow area. For boiling bubbles, heat transfer causing the continuous growth of the bubble is superimposed on the oscillating boundary layer development in the liquid adjacent to the interface. Solutions were either numerical or approximate. Rectified heat transfer was predicted [26. 27]. Rectified heat transfer is the net effect of a decrease of the heat transfer during the half cycle when the bubble contracts and an increase during the other half cycles. The increase exceeds the decrease. As a result, rectified heat transfer to free bubbles is a net increased heat transfer. A nice experimental study of rectified heat transfer with phase-change was presented by Shpak *et al.* [28]. The

additional energy flux corresponding to rectified heat transfer was shown to be proportional to the relative radial displacement squared. The combination of heat transfer and oscillations of a constraint bubble, such as a boiling bubble, has to the best of my knowledge not been studied so far.

Despite the fact that the Rayleigh-Plesset equation is often used, it is seldom realized that it is only one of a set of Euler-Lagrange equations that govern the dynamics of bubble or drop oscillation. The Euler-Lagrangian approach was already studied in the context of bubble motion in the 19th century [1]. The main advantages of this approach are a strong reduction of the number of parameters for which the dynamics need to be predicted and an analytical solution except for time integration. Generalization and physical interpretation of results obtained by other means, such as numerical studies, is facilitated by the Euler-Lagrange approach. This approach will therefore be used in this paper to study various aspects of boiling bubble deformation and oscillation.

Amongst the topics covered by this paper are:

- the conversion of arbitrary large-amplitude bubble deformation into isotropic deformation
- the occurrence of resonance cases in which this conversion is amplified
- the existence of resonance cases in which several different bubble sizes at a time are excited

The Euler-Lagrange approach presented will be seen to provide a full solution of the dynamics of an axisymmetric bubble which deforms with large amplitude oscillations. In addition, a perturbation analysis is carried out that allows for simplified solutions that increase our physical understanding while providing predictions of resonance frequencies. In particular, the effects of finite amplitude oscillation and the proximity of the wall will be investigated.

Boiling heat transfer augmentation by acoustics has been proven to occur [29]. To the best of our knowledge, none of these experiments utilized low-amplitude at predicted resonance frequencies of bubbles. Whether appropriate acoustic excitation promoted detachment and affect the boiling bubble detachment size has been investigated in a recent study of which some findings will be reported [30].

No experiments have been found in the literature that report large amplitude oscillations of a boiling bubble attached to a wall during many oscillation cycles. Growth of vaporized bubbles under normal conditions is that fast that detachment occurs in a time typically of the order of 10 ms [31]. An experimental study will be reported in which large-amplitude oscillation of a boiling bubble with a foot at a plane wall has been realized during about 180 s. The physical nature of the oscillations will be examined.

NONLINEAR MODEL OF BUBBLE DEFORMATION

Modeling assumptions

A single boiling bubble in an infinite liquid volume is considered. The bubble may be free, *i.e.* very remote from any wall, or in the vicinity of a plane wall, or attached to the plane wall. The free bubble is considered first and no examples of bubbles attached to a wall will be given in the present paper. Deformation is generally that large that a full nonlinear solution is required. Both a general method and an approximate solution, in terms of an expansion, will be presented. First cases without sound excitation will be considered and thereafter anisotropic bubble deformation with the influence of a sound wave of frequency $\nu = 1/T_w$ is predicted. The following assumptions are made:

1. Heat transfer to the bubble is such that slow growth on a time scale large as compared to the oscillation period T_w occurs
2. The initial shape is simple, which means either spherical, with radius R_0, or described by $b_0 + b_3P_3\cos(\theta)$ in a polar coordinate system with polar angle θ and with P_3 the Legendre polynomial of order 3. The initial pressure inside the bubble, p_0, is homogeneous and given by $p_\infty + 2\sigma/R_0$., where σ is the surface tension coefficient and p_∞ the imposed pressure at far distance from the bubble
3. The wavelength of the sound wave, λ , is much larger than radius R_0, whence the imposed sound wave is felt by the bubble as a homogeneous pressure oscillation.
4. Viscous damping is negligible on the time scale $10T_w$ or can be overestimated by Levich drag.
5. The content of the bubble is vapor that behaves as a perfect fluid; there is no inert gas.
6. The vapor-liquid interface is at thermodynamic equilibrium.
7. Surface active agents are absent.

Because of assumption 4, fluid motion can be taken to be irrotational. According to Lamb[20] (p. 641) and Longuet-Higgins[21] (p. 552) this is possible when R_0 satisfies

$$(R_0(k-2)k(k+1))^{1/4} \gg (4\mu^2/(\rho_L\sigma))^{1/4} \quad (1)$$

for any integer k in excess of 2. Here, μ is the dynamic viscosity of the liquid and ρ_L its mass density. For boiling of water at ambient pressure, the right-hand-side (RHS) of (1) amounts 0.0089 which is less than the left-hand-side (LHS) by a factor 30 for the most critical k-value of 3 and R_0 = 0.5 mm. For a factor 10, R_0 should be exceeding 5 μm. All bubbles considered below satisfy these requirements easily.

The bubble pressure, p_b, is taken to be homogeneous (assumption 2) and the vapor is assumed to behave as a perfect gas (5), but the mass density and the temperature might be non-uniform inside the bubble. The homobaricity of the vapor is by Nigmatulin[22] (p. 168) shown to be satisfied when typical vapor velocities are much less than the speed of sound and high-frequency variations of the velocity do not occur. This condition is satisfied in a broad class of problems.

When T_w would become comparable to the time for molecular relaxation or when the vapor Mach number is about 1, thermodynamic non-equilibrium would occur, in conflict with assumption 6. According to Gumerov[23,24], this is not the case when

$$8\pi^2(\gamma-1)k_v T/(T_w \sigma_{hkls}^2 \gamma \rho_v \Delta h^2) \ll 1 \quad (2)$$

where σ_{hkls} is the so-called accommodation coefficient of the Herz-Knudsen-Langmuir-Schrage equation; γ is the ratio of heat capacities, k_v is the heat conduction coefficient, ρ_v the mass density of the vapor and Δh the enthalpy of evaporation.

For sound frequencies of the order of 1 kHz and values of σ_{hkls} of the order of 0.01 or higher assumption 6 is fully satisfied.

Evolution equation for the content of a deforming bubble

When a bubble is oscillating and growing, its content (vapor) experiences a process that can be determined from the energy equation. First the case of an isotropic, deforming bubble is considered. Nigmatulin[22] (p. 175) integrates the energy equation to find a relation (his Eq. (2.4.33)) between the velocity of the vapor at the interface, $v_v(R)$, and the vapor velocity, v_v, at arbitrary radial distance, r. Let c_p be the specific heat capacity with constant pressure of the vapor. Upon taking the latter to be the center of the bubble, the following equation for the velocity of the vapor at the location of the interface is easily derived. It is Eq. (6) given by Hao & Prosperetti[25]:

$$v_v(R) = \{(\gamma - 1)\, k_V\, \partial T_v/\partial r - \tfrac{1}{3}\, R\, dp_v/dt\} / (\gamma p_v) \qquad (3)$$

Here, T is temperature, t time, suffix v indicates vapor, k heat conduction coefficient, γ denotes c_p/c_v of the vapor which has a gas constant equal to the difference $c_p - c_v = c_p(1-1/\gamma)$ and satisfies

$$\rho_v\, T_v = p_v / (c_p - c_v). \qquad (4)$$

The evaporation rate, $\hat{w}$, is the mass flow rate across the interface and is given by

$$\rho_v (\dot{R} - v_v(R)) = \hat{w} = \{\, k_L\, \partial T_L/\partial r|_R \; - \; k_V\, \partial T_v/\partial r|_R \,\} / h_{LV} \qquad (5)$$

where $\dot{R}$ denotes velocity of the interface, dR/dt, suffix L denotes liquid and h_{LV} is the enthalpy of evaporation. The combination of (3) and (4) gives Eq. (9) of Hao & Prosperetti[25], which we prefer in the following form:

$$\mathrm{d}\, ln\, V_b/\mathrm{d}t + \mathrm{d}\, ln\, p_v^{1/\gamma}/\mathrm{d}t = (3/R)\, \{1/(\rho_v(T_s)\, h_{LV})\}$$
$$(\, k_L\, \partial T_L/\partial r|_R - \{1 - h_{LV}/\, (c_{p,V}\, T_s)\, \}\, k_V\, \partial T_v/\partial r|_R) \qquad (6)$$

Here, V_b denotes the bubble volume. The advantage of this form (5) is that the governing equation is easily seen to reduce to the Poisson equation, $p_v.V_b^{\gamma} \equiv$ constant, in case the process is adiabatic.

For the more general case of a deforming bubble, it is convenient to introduce the brackets $< >$ to denote averaging over the entire bubble surface, as done by van der Geld *et al.*[26]. For example, $<\hat{w}> = <\rho_v\, \boldsymbol{n}.(\boldsymbol{v}_I - \boldsymbol{v}_v)>$ is given by

$$< \hat{w} > \equiv (1/A_b) \iint \hat{w}\, dA = \rho_v(T_s)(1/A)\, \mathrm{d}V_b/\mathrm{d}t \; -$$
$$\rho_v(T_s) < \boldsymbol{n}.\boldsymbol{v}_v > \qquad (7)$$

where A_b is the area of the bubble surface, suffix s indicates saturation value, $\boldsymbol{v_I}$ is the velocity of the interface and $\boldsymbol{n}$ the outward normal to the interface. The expression on the right-hand-side (RHS) of (7) follows from $\hat{w} = \rho_v\, (v_I - v_v(R))$. The average value of the normal component of the vapor velocity, $<\boldsymbol{n}.\boldsymbol{v}_v>$, is eliminated with the aid of the following expressions for $<\hat{w}>$:

$$<\hat{w}> = (< k_L\, \boldsymbol{n}\cdot\boldsymbol{\nabla} T_L > - < k_V\, \boldsymbol{n}\cdot\boldsymbol{\nabla} T_V >) / h_{LV}.$$

The derivation closely follows the one leading to (6) and the following equation for the process of heat and mass transfer to the content of a deforming bubble is found to be valid:

$$\mathrm{d}\, ln\, V_b/\mathrm{d}t + \mathrm{d}\, ln\, p_v^{1/\gamma}/\mathrm{d}t = (A_b/V_b)\, \{1/(\rho_v(T_s)\, h_{LV})\}$$
$$(< k_L\, \boldsymbol{n}\cdot\boldsymbol{\nabla} T_L > - \{1 - h_{LV}/\, (c_{p,V}\, T_s)\, \} < k_V\, \boldsymbol{n}\cdot\boldsymbol{\nabla} T_V >) \qquad (8)$$

The bubble surface area is denoted with A_b and $\boldsymbol{n}\cdot\boldsymbol{\nabla}$ is the gradient in direction normal and outward to the bubble surface. By above assumption 1, the RHS of (8) can be taken to be zero on the timescale of a couple of pressure oscillations. In this near-adiabatic case of a deforming bubble the Poisson equation is recovered. Note that the vapor temperature is only assumed to have the saturation value, T_s, at the vapor-liquid interface.

Generalized forces for capillarity and hydrostatic pressure

A convenient way to predict motion and arbitrary deformation of a fluid sphere near a wall is offered by the Euler-Lagrange formalism[28,29,30]. This approach yields a coupled set of nonlinear second order differential equations that control bubble dynamics. The generalized forces necessary in this formalism are derived by integration of the mechanic energy balance, which makes all force expressions unambiguous. First, the dominant forces, those due to gravity and surface tension, are considered.

When generalized coordinates, b_j, numbered by positive integer j, are used, Newton's law of motion has to be transformed and expressions for the corresponding generalized forces, F_j, have to be derived. This has been done in a derivation that starts from the so-called mechanical energy balance for the fluid surrounding the bubble[9]. The resulting time rate of change of the kinetic energy in the fluid, T, can be given the form

$$\frac{dT}{dt} = \sum_j F_j\, \dot{b}_j\,, \qquad (9)$$

where the generalized velocities are denoted with $\dot{b}_j = db_j/dt$. Each F_j represents a generalized force that corresponds to a generalized coordinate b_j. There is no restriction on kinetic energy T in this stage; it accounts for turbulence as well as for creeping flow in a way that will be discussed in the next subsection below. Terms related to energy dissipation are proportional to the dynamic viscosity of the liquid, μ_L, and yield drag forces, F_j^{drag}, which are only nonzero in case of nonzero velocity gradients. Terms related to gravity yield gravity forces, F_j^g. When the connection is made between the pressure in the liquid, p_L, and the homogeneous pressure in the bubble, p_v, also capillary forces, F_j^{σ}, and forces $F_j^{\Delta p}$ related to the overpressure in the bubble, $\Delta p = p_v - p_L$, can be distinguished. Here, pressure p_L is the hydrostatic pressure in the fluid at the lowest part of the bubble or at the solid plane wall on which the bubble is footed. The overpressure inside the bubble is related to heat transfer, see (8). In measurements, the temperature field around the bubble is often unknown and also the overpressure is then unknown. The fact that Δp occurs in each governing Euler-Lagrange equation may promote assessment of Δp from measurement data[31]. For each positive integer j, the sum $(F_j^{\sigma} + F_j^{\Delta p})$ results from the sum $(\Delta p\, dV_b/dt$

$+ \sigma\, dA_b/dt$), where volume and vapor-liquid interfacial area of the bubble are V_b and A_b, respectively. If the bubble has a part in contact with a solid wall, *i.e.* a bubble foot, an additional capillary term related to the Helmholtz free energy of the solid-liquid interface occurs in (9). The overpressure force components, $F_j^{\Delta p}$, follow from

$$F_j^{\Delta p} = \Delta p\, \partial V_b / \partial b_j$$

The overpressure, capillary and gravitational forces originate from integrals over the gas-liquid interface. The surface integrals over the gas-liquid interface mostly can be expressed in quantities prevailing at the bubble foot. The latter quantities are familiar from other derivations of forces acting on a bubble[31].

Generalized forces for fluid dynamics

For the cases without sound in the fluid it can be assumed that the fluid flow is solenoidal which is for example satisfied if the fluid is incompressible. The rate dT/dt can be written as the sum of the time rates of change of a purely irrotational component, T^{irrot}, of a purely vector potential component, T^{vort} and of a mixed component, T^{mixed}. This is because the velocity field is the sum of an irrotational component and a solenoidal vector potential component [12]. Added mass coefficients ψ_{ij} are defined such that

$$2T^{irrot}/(\rho_L V_b) = \sum_{i,j=1} \psi_{ij}\ \dot{b}_i\ \dot{b}_j\ . \qquad (10)$$

The added mass forces and added mass coefficients stay the same in viscous flows[32]. The added mass coefficients retain their value also if vorticity is present and have therefore a general validity. The Euler-Lagrange equation corresponding to, for example, b_3 reads

$$\frac{d}{dt}\frac{\partial T^{irrot}}{\partial \dot{b}_3} - \frac{\partial T^{irrot}}{\partial b_3} = F_3^{\sigma} + F_3^{\Delta p} + F_3^{g} + F_3^{drag} + F_3^{vort} \qquad (11)$$

where the vorticity contribution, connected to T^{vort}, is put in F_3^{vort}. If a bubble foot is present, a uniform approaching flow with velocity V parallel to the wall yields a potential flow lift contribution to the force balance in the direction perpendicular to the solid wall. Lift and other hydrodynamic forces are further discussed below. If the left-hand-side (LHS) of (11) is named $-F_3^{inertia}$, the force balance for the component b_3 takes the following form:

$$-F_3^{inertia}(b_j,\ \dot{b}_j\ ,\ddot{b}j\ ) = F_3{}^{\sigma}(b_j) + F_3{}^{\Delta p}(b_j) + F_3{}^{g}(b_j) + F_3{}^{drag}(b_j,\ \ddot{b}j\ ) + F_3{}^{vort}(b_j,\ \dot{b}_j\ ) \qquad (12)$$

Here, the occurrence of $(b_j,\ \dot{b}_j\ ,\ \ddot{b}j\ )$ indicates dependency on all generalized coordinates, generalized velocities and generalized accelerations. The hydrodynamic force $F^{inertia}$ is computed from potential flow theory. This inertia force is linear in the generalized velocities. Viscous effects in the absence of surface-active agencies (see assumption 7 above) can often be accounted for by the so-called Levich approach[26,30,31]. Because of fast growth of a boiling bubble, for example, free vorticity in the boundary layers is negligible in this case, and the Levich approach gives an appropriate overestimation[26].

Governing equations and generalized coordinates

If index *3* in (12) is replaced by arbitrary index *k*, a set of coupled second order differential equations in the generalized coordinates is obtained. This set of equations can be given the form of a symmetric matrix of added mass coefficients, $\boldsymbol{A}$, acting on a column vector of the second order derivatives of generalized coordinates and equalling a column vector, $\boldsymbol{c}$, comprising all driving forces, the generalized velocities and coordinates but no generalized accelerations (Eq. (2.19) of [27]):

$$\boldsymbol{A}\cdot\ddot{\boldsymbol{y}} = \boldsymbol{c}, \qquad (13)$$

where $\ddot{\boldsymbol{y}}$ denotes the column-vector $(\ddot{b}_1, \ddot{b}_2, \ddot{b}_3, \ddot{b}_4, ...)^T$. The diagonal, first off-diagonal row and the first two rows (and columns) of $\boldsymbol{A}$ are usually significant. Each row-equation of (13) corresponds to an Euler-Lagrange equation of the form (11) or (12). The set (13) is integrated in time, the only numerical step involved. To be able to interpret the equations (13) physically, first the generalized coordinates need to be specified. This is done in the following important example.

Consider an axisymmetric, freely deforming bubble in an infinite liquid or a semi-infinite liquid bounded by a plane wall. The time-dependent coefficients $b_m(t)$ in the expansion of the function $R(\theta, t)$ that describes the interface:

$$R(\theta, t) = \sum_m b_m(t)\, P_{m-1}(\cos\theta) \qquad (14)$$

are the generalized coordinates. Angle θ is the polar angle defined to be zero at the top of the bubble furthest away from the wall and the P_{m-1} are the Legendre polynomials. Integer m is positive and nonzero and counts the coefficients. In principle, an infinite amount of coefficients is needed but in practice 40 coefficients describe complex deformation already. Coefficient b_2 corresponds to motion of the bubble as a whole. Instead of b_2, often the distance h of the centre of the bubble to a plane wall is used. Without loss of generality only initial shapes will be considered for which b_1 and b_3 are nonzero. The significance of the first two rows in $\boldsymbol{A}$ of (13) implies that with each excitation of b_3 mode of a bubble near the wall, also the first isotropic mode (b_1) and the distance h are affected. For excitation of normal modes other than b_3 similar results hold.

The breathing mode: extended Rayleigh-Plesset equation

Of particular interest is the extended Rayleigh-Plesset equation that is connected to isotropic deformation, b_1, and the first row-equation of (13); this is the so-called breathing mode. In the case of general deformation without a wall it reads[33]

$$2\psi_{11}\ddot{b}_1 + 2\sum_{k=3}\psi_{k1}\ddot{b}_k = 2\,Q_1/\rho_L - \dot{b}_1^2\,\partial\psi_{11}/\partial b_1 - 2\dot{b}_1\sum_{k=3}\dot{b}_k\,\partial\psi_{11}/\partial b_k + \sum_{k,m=3}\dot{b}_k\,\dot{b}_m\,\partial\psi_{mk}/\partial b_1 - 2\sum_{k,m=3}\dot{b}_k\,\dot{b}_m\,\partial\psi_{m1}/\partial b_k \qquad (15)$$

Here, Q_1 is the sum of generalized forces $F_1^{\sigma} + F_1^{\Delta p} + F_1^{g} + F_1^{drag} + F_1^{vort}$. The Euler-Lagrange equation for the anisotropic deformation component b_3 in the proximity of a plane wall is given by Eq. (3.15) of ref [27]. It exhibits a direct coupling of b_3 with b_1 and h.

Equation (15) shows that in the full nonlinear solution of bubble deformation at each instant of time many derivatives of added mass coefficients need to be assessed. In [33] it is shown that not close to the wall quite some added mass coefficients have only a negligible contribution. Linearization of the set of governing equations (13) gives oscillatory solutions at frequencies which are named eigenmodes. The oscillations result from a trade-off between kinetic energy, represented by the added mass coefficients, and potential energy related to the Helmholtz free energy of the surface (van der geld & Kuerten[27], page 291). Energy related to pressure in the bubble normally only contributes to the high-frequency oscillations but it will not be neglected below.

The generalized Rayleigh-Plesset equation (15) controls the breathing mode in the presence of arbitrary deformation. If extended with b_2 or h, this equation easily explains the well-known Bjerknes forces between two spheres. In the solution method, an identical mirror bubble accounts for the presence of a plane wall. Volume oscillations of one pulsating sphere radiate a velocity field that creates kinematic buoyancy at the place of the other sphere. Averaged over many pulsation cycles the spheres are attracted to one another. Obviously, the Bjerknes force promotes coalescence.

A bubble far away from a wall and undergoing a process described by (6) with a negligible RHS, a so-called Poisson process, possesses a natural frequency corresponding to isotropic deformation, $\omega_{RP} = 2\pi / T_{RP}$, which is given by

$$\omega_{RP}^2 = 3\gamma p_\infty / (\rho_L R_{00}^2) + 2(3\gamma - 1)\, \sigma / (\rho_L R_{00}^3) \qquad (16)$$

This frequency will be named the Rayleigh-Plesset frequency (RP-frequency) because it originates[27] from the Rayleigh-Plesset equation (15). Bubble radius R_{00} is a reference radius, usually equal to an initial radius of the bubble process and pressure p_∞ is the system pressure in the liquid, far away from the bubble. Close to a plane wall the RP-frequency is a function of distance to the wall and of the added mass coefficient corresponding to motion perpendicular to the wall[27]. In the vicinity of the wall the RP-frequency is reduced by a factor 1.2.

Approximate solutions often facilitate physical interpretation of the bubble dynamics, like in the above example of a trade-off of potential and kinetic energies. Since full solutions exhibit features which differ strongly from the linear approximations and which are important for a proper understanding of the physics involved, other approximations are investigated in the subsequent section. Amongst the concrete results of the perturbation analysis to be performed are resonance frequencies and the effect of finite disturbance amplitude on resonance frequencies. These findings will become useful in the selection of acoustic frequencies to excite boiling bubbles and in the setting up of dedicated validation experiments.

EFFECT OF AMPLITUDE ON OSCILLATION FREQUENCY

Approximate solution for anisotropic deformation without a wall

For reasons indicated above, a perturbation analysis is now used to produce approximate nonlinear solutions. Note that only a single set of parameters, the generalized coordinates, needs to be perturbed which lead to a consistent and coherent solution of which the accuracy is readily assessed by comparison with the full nonlinear solution described in the previous sections.

In this section, shape oscillations induced by an initially non-spherical shape will be studied. Without loss of generality only the coefficients b_1 and b_3 will be taken to be nonzero initially. Any b_k for odd k could have been selected, but since bubble shape oscillations measured in our lab show clear b_3-based deformation this value for k was selected. A perturbation analysis with $\beta = b_3(0)/b_1(0)$ as small parameter will be performed. The initial radius $R_0 = b_1(0)$ is used to render the time-dependent functions b_{12}, b_{31}, … dimensionless in the following defining equations:

$$\begin{aligned} b_1/R_0 &= 1 + \beta\, b_{11} + \beta^2 b_{12} + \beta^3 b_{13} \\ b_3/R_0 &= \beta\, b_{31} + \beta^2 b_{32} \\ b_5/R_0 &= \beta\, b_{51} \end{aligned} \qquad (17)$$

Because of lack of a preferential direction the bubble deforms symmetrically with respect to the equatorial plane through its center, whence all even numbered coefficients b_2, b_4, … are zero. By definition of β, $b_{31}(0)=1$, $b_{32}(0) = 0 = b_{11} = b_{12} = \ldots$. The bubble will be taken to be at rest initially. The initial generalized velocities are therefore all zero. The initial pressure in the bubble, p_0, is taken to exceed that in the liquid at infinity, $p_{L,\infty}$, by $2\sigma / R_0$. The offset in initial pressure due to the nonzero initial value of b_3 will be seen to cause a slight initial expansion of the sphere which is irrelevant for the deformation characteristics at later times under study.

The driving forces contain derivatives of the surface area of the bubble, A_b, with respect to the generalized coordinates. Because of axisymmetry, the radial component of the normal, n_r, is a function of polar angle θ only. It can be expanded in Legendre polynomials as follows:

$$n_r = \sum_{j=1} g_j P_{j-1}(\cos(\theta)). \qquad (18)$$

To lowest orders in β the following approximations can be derived:

$$\begin{aligned} g_1 &= 1 + \beta^2 \{(45/2)\, b_{51}^2 - (15/2)\, b_{31} b_{51} - (3/5)\, b_{31}^2\} \\ g_3 &= (3/28)\, \beta^2 \{675\, b_{51}^2 - 260\, b_{31} b_{51} - 4\, b_{31}^2\} \\ g_5 &= (3/35)\beta^2 \{425\, b_{51}^2 - 200\, b_{31} b_{51} + 12 b_{31}^2\} \end{aligned} \qquad (19)$$

while even numbered coefficients g_2, g_4, … are zero for sake of symmetry. Similarly,

$$1/n_r = \sum_{j=1} h_j P_{j-1}(\cos(\theta))$$

with a coefficient-vector $\{h_k\}$ that is readily assessed as $inv(E).(1, 0, 0, 0, \ldots)^T$, with matrix element E_{ij} given by $\sum_q g_q e_{qij}$. The structural coefficients e_{ijk} defined by

$$P_{i-1}.P_{j-1} = \sum_k e_{ijk} P_{k-1} \qquad (20)$$

are rational functions that are transforms of the Celbsch-Gordan coefficients. Derivatives of A_b that occur in the driving forces are

$$\partial A_b/\partial b_3 = 2\pi R_0\{(2/5)\sum_{k,m=1} b_k e_{km3}(h_m + g_m) + 2\sum_{sj} b_s \Omega_{sj} g_j\}$$

$$\partial A_b/\partial b_1 = 2\pi R_0\{\sum_k (2/(2k-1))b_k (h_k + g_k)\} \quad (21)$$

where matrix $\{\Omega_{sj}\}$ is an expression in terms of the structural constants, e_{ijk}. To lowest orders in β, $(\partial A_b/\partial b_3)/(\pi R_0)$ is given by

$$\left(-\frac{348}{35}b_{31}^3 - \frac{9998}{63}b_{31}b_{51}^2 + \frac{156}{7}b_{51}b_{32} - \frac{312}{7}b_{51}b_{11}b_{31} + \frac{24}{35}b_{31}b_{32} - \frac{24}{35}b_{11}b_{31}^2 + \frac{3113}{105}b_{31}^2 b_{51} + \frac{13205}{36}b_{51}^3 + \frac{810}{7}b_{11}b_{51}^2\right)\beta^3 + \frac{32}{5}b_{32}\beta^2 + \frac{32}{5}b_{31}\beta$$

and $(\partial A_b/\partial b_1)/(\pi R_0)$ is given by

$$\left(8b_{13} + \frac{546}{5}b_{31}^2 b_{51} + 30b_{51}b_{32} - 60b_{51}b_{11}b_{31} + 180b_{11}b_{51}^2 + \frac{24}{5}b_{31}b_{32} - \frac{24}{5}b_{11}b_{31}^2 + \frac{945}{4}b_{51}^3 - \frac{42}{5}b_{31}^3 - 315b_{31}b_{51}^2\right)\beta^3 + 8\beta^2 b_{12} + 8\beta b_{11} + 8$$

The last expression contains $8b_1$ plus third order terms in β. The above expression for $(\partial A_b/\partial b_3)/(\pi R_0)$ contains $(32/5)b_3$ plus third order terms in β.

It is convenient to express $(p_b - p_L)/\rho_L$ in terms of two radian frequencies, ω_L and ω_{RP}, that are defined by:

$$\omega_L^2 = 12\sigma/(\rho_L R_0^3)$$
$$\omega_{RP}^2 = (3\gamma p_L + 2(3\gamma - 1)\sigma/R_0)/(\rho_L R_0^2)\,. \quad (22)$$

This yields for $(p_b - p_L)/(R_0^2\rho_L)$:

$$\frac{1}{6}\omega_L^2\left(\frac{V_{b0}}{V_b}\right)^\gamma + \left(\omega_{RP}^2\frac{1}{3\gamma} - \omega_L^2\left(\frac{1}{6} - \frac{1}{18\gamma}\right)\right)\left(\left(\frac{V_{b0}}{V_b}\right)^\gamma - 1\right)$$

Here, V_{b0} is the initial volume. Volume V_b and its derivatives with respect to b_1, b_3 and b_5 follow from

$$V_B/(4\pi/3) = b_1^3 + (3/5)b_1 b_3^2 + (2/35)b_3^3 + (6/35)b_3^2 b_5 + (1/3)b_1 b_5^2 \quad (23)$$

The Euler-Lagrange equation corresponding to b_3 can be written as

$$\psi_{33}\ddot{b}_3 + \psi_{13}\ddot{b}_1 + \psi_{53}\ddot{b}_5 = Q_3/(\rho_L V_b) - \tfrac{1}{2}\dot{b}_3^2\frac{\partial\psi_{33}V_b}{V_b\partial b_3} - \dot{b}_1\dot{b}_3\frac{\partial\psi_{33}V_b}{V_b\partial b_1} - \dot{b}_1^2\frac{\partial\psi_{13}V_b}{V_b\partial b_1} - \dot{b}_1^2\frac{\partial\psi_{11}V_b}{V_b\partial b_3} - \dot{b}_3\dot{b}_5\frac{\partial\psi_{33}V_b}{V_b\partial b_5} \quad (24)$$

Similar to Q_1 in (15), Q_3 is the sum of generalized forces $F_3^\sigma + F_3^{\Delta p}$ if gravity, drag and forces due to vorticity are negligible. The added mass coefficients can be expressed[33,34] in terms of components of the inverse of an operator, G_{ij}, which are polynomials in the $\{b_k\}$. The ψ_{ij} are therefore rational functions of the generalized coordinates, be it lengthy expressions in general.

The full solutions of the previous sections show that most of the time the diagonal, first off-diagonal and the first two rows of the matrix $\boldsymbol{A}$ are significant. This implies that dispersion of a normal mode is limited to the breathing mode, *i.e.* b_1, to h and to neighboring modes. If for example b_7 would have been excited, the b_5 and b_9 modes would have been found to be rapidly growing while the other modes are mainly excited via the isotropic b_1 mode. In the b_3-case at hand, the perturbation analysis with the full expressions for the added mass coefficients shows that the coupling terms involving b_5 are relatively small; only b_{51} will be considered in the following. The analysis also yields $b_{11} = 0$. With these results the added mass coefficient $\psi_{31} = \psi_{13}$ in lowest order of the perturbation parameter β can be written as:

$$\beta\{b_{31}(t) + 2\beta b_{31}(t)^2/35 + \beta b_{32}(t)\} \quad (25)$$

while ψ_{35} is given by:

$$-\beta\{18 b_{31}(t)/175 + 2952\beta b_{31}(t)^2/13475 + 18\beta b_{32}(t)/175\} \quad (26)$$

An added mass coefficient that is not proportional to β is ψ_{33}:

$$\frac{1}{5} + \frac{4}{35}b_{31}(t)\beta + \frac{442}{1225}\beta^2 b_{31}(t)^2 + \frac{4}{35}\beta^2 b_{32}(t) \quad (27)$$

Since b_{11} is zero, the two terms with $\dot{b}_1^2$ on the RHS of the Euler-Lagrange equation corresponding to b_3, Eq. (24), are proportional to β^4 and not contributing to terms which are lowest order in β. The term in (24) comprising $\dot{b}_3$ turns out to be small. The two other terms with derivatives of added mass coefficients are $\dot{b}_1\dot{b}_3\frac{\partial\psi_{33}V_b}{V_b\partial b_1}$ and $\dot{b}_3^2\frac{\partial\psi_{33}V_b}{V_b\partial b_3}$ which can be expanded, respectively, as

$$(-735 b_{12} + 148 b_{31}^2 + 280 b_{32})\beta^2/(1225 R_0) + 8 b_{31}\beta/(35 R_0) + 3/(5R_0)$$

$$(-490 b_{12} + 1626 b_{31}^2 + 4123 b_{32})\beta^2/(8575 R_0) + 1178 b_{31}\beta/(1225 R_0) + 4/(35R_0).$$

Both expansions contain a homogeneous term, *i.e.* one without β, and are therefore significant.

The perturbation analysis boils down to equating terms with equal power of β. For b_{31} this yields a differential equation which has only one solution if the initial conditions are employed:

$$b_{31} = \cos(\omega_L t). \quad (28)$$

If terms involving b_5 are taken along, the perturbation analysis gives the following equation for b_{32}:

$$-\frac{5}{3}\omega_L^2 d_3\cos(\omega_L t)b_{51}(t) + \left(-\frac{3}{7}\omega_L^2 - \frac{5}{4}\omega_L^2 d_2\right)\cos(2\omega_L t) + \frac{d^2}{dt^2}b_{32}(t) - \frac{5}{4}\omega_L^2 d_2 - \frac{1}{7}\omega_L^2 + \omega_L^2 b_{32}(t)$$

The constants d_2 and d_3 are 2/35 and 6/35, respectively. The solution for b_{32}, without the b_{51}-term, is:

$$3/14 - cos(\omega_L t)/21 \; - cos(2\,\omega_L t)/6 \qquad (29)$$

This solution explains, in a way described below, the remarkable experimental finding that the radian frequency of an oscillating globe appears to be decreasing with increasing value of the initial amplitude, *i.e.* with increasing β. A summary of some of these experimental results is given by Tsamopoulos & Brown [11, page 535]. The present solution

$$\beta\, cos(\omega_L t) + \beta^2 \{(3/14) - cos(\omega_L t)/21 - cos(2\,\omega_L t)/6\}$$

can be expanded as

$$\beta\, cos(\omega_L t) + \beta^2 \{(5/14)\,(\omega_L t)^2 - (19/168)\,(\omega_L t)^4 + \ldots\} \qquad (30)$$

To the same order of powers of $\omega_L t$, the expansion of $cos((1 - \frac{5}{14}\beta)\,\omega_L t)$ is

$$\beta\, cos(\omega_L t) + \beta^2 \{(5/14)\,(\omega_L t)^2 - (10/168)\,(\omega_L t)^4 + \ldots\} \qquad (31)$$

This shows that for times small enough for the $(\omega_L t)^4$-term to be relatively unimportant $b_3/(\beta R_0)$ is well described by

$$cos(\{1 - \tfrac{5}{14}\beta\}\,\omega_L\, t). \qquad (32)$$

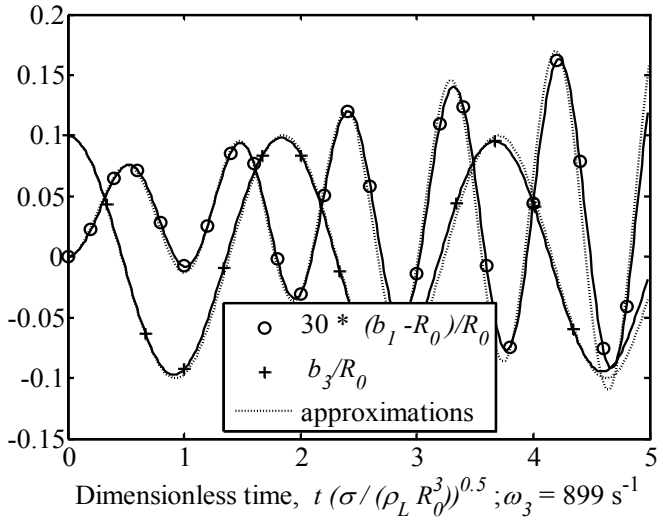

Figure 1 Shape coefficient histories at early times for b_3-excitation with $\beta = 0.1$, $\gamma = 1.4$ and $p_L R_0/\sigma = 10.89$, *i.e.* $k = 1.1$.

The above solution (32) shows that if b_3 is approximated by

$$b_3 \approx \beta \cos(\varpi_3\, t), \qquad (33)$$

ϖ_3 becomes dependent on amplitude β. This is in agreement with the findings of both experiments and previous analysis, see the summarizing Fig. 4 of Tsamopoulos & Brown (1983, page 535). It also explains why the approximation for b_3 given by Eq. (9) in Fig. 1 deviates from the full solution; the value of ϖ_3, given in the caption, is obtained by fitting to the first cycle of the full solution of b_3. If ω_L would have been used, the agreement would have been slightly worse.

Approximate nonlinear solution for isotropic deformation without a wall

The derivation of the above results for b_3 required the simultaneous solving for b_1. Let ω_3 be equal ω_L ; each normal frequency ω_n is proportional to[33] ω_L and for ω_3 the proportionality constant is 1. The perturbation analysis shows that the breathing mode is described by

$$(b_1 - 1)/R_0 = A\,\beta^2 \{\cos(2\,\omega_3\, t) - \cos(\omega_{RP}\, t)\} + B\,\beta^2 \{\cos(\omega_{RP}\, t) - 1\} \qquad (34)$$

with ω_{RP}^2 given by (16) and

$$A = 0.2\{\omega_{RP}^2 - (17/6)\omega_3^2\}/(4\omega_3^2 - \omega_{RP}^2)\,; \quad B = -0.2\{\omega_{RP}^2 + \omega_3^2/2 + \omega_L^2/3\}/\omega_3^2 \qquad (35)$$

The occurrence of the term with ω_L in B stems from the initial condition of the pressure in the bubble, p_b. Despite the initial deformation, prescribed by $\beta = 0.1$, the initial value of p_b has been chosen to be $p_L + 2\sigma/R_0$, *i.e.* the equilibrium value of a sphere with radius R_0. The actual equilibrium pressure, minus p_L, is given by 2σ divided by the radius of the volume-equivalent sphere of the initial bubble. Since this radius is larger, the mean value of b_1/R_0 is found to exceed 1, see Fig. 1. The physics of an initial offset in pressure leads to an extra ω_L-term in the generalized b_1-force (gravity, drag and vorticity are neglected), Q_1:

$$Q_1/(4\pi\,\rho_L \beta^2) = -\,\omega_{RP}^2\, b_{1,2} + \omega_{RP}^2\, 0.2\, \sin(\omega_3\, t)^2 + 0.2\,\omega_L^2/6 \qquad (36)$$

Equation (36) is accurate up to order β^2. The governing equation of b_1, an extension of the Rayleigh-Plesset equation, reads

$$b_1^3\, \ddot{b}_1 + b_1^2\, b_3\, \ddot{b}_3\, \{(1/3) + (b_3/b_1)/7\} + b_1^2\, \dot{b}_3^2\, ((7/30) - (b_3/b_1)/105) = Q_1/(4\pi\,\rho_L) \qquad (37)$$

The terms with the ratio (b_3/b_1) in equation (37) are insignificant to the present level of approximation, but contribute to $b_{1,3}$. Equations (36) and (37) lead to the solution given by Eq. (34), and the last term on the RHS of Eq. (36) for Q_1 leads directly to the ω_L-term in B of (35).

The approximate line for b_1 in Fig. 1 has been obtained by fitting ϖ_3 to the first part of the full solution of b_3 and using the value thus obtained for ω_3 in Eq. (34). This procedure will be named the approximating of b_3 with Eq. (33). The accuracies of the approximations (33) and (34) can be seen in this Fig. 1. When computations are performed with $\beta = 0.001$ and smaller, nearly perfect agreement between Eq.'s (33) and (34) and full nonlinear solutions is obtained. This shows that discrepancies in Fig. 1 are due to higher order terms in β.

The perturbation analysis yields expressions for added mass coefficients related to b_1, and their derivatives, similar to those given above. It also yields the already used $b_{11}(t) = 0$ and the following equation for $b_{12}(t)$:

$$\frac{d^2}{dt^2}\, b_{12}(t) - a_3 \sin(\omega_L\, t)^2\, \omega_L^2 + a_1 \cos(\omega_L\, t)^2\, \omega_L^2 - \frac{1}{5}\,\omega_{RP}^2 + \frac{1}{5}\,\omega_{RP}^2 \cos(\omega_L\, t)^2 + \omega_{RP}^2\, b_{12}(t) + \frac{1}{3}\,\omega_{RP}^2\, d_4\, b_{51}(t)^2 - \frac{1}{30}\,\omega_L^2$$

The constants d_4, a_1 and a_3 are 1/3, −1/3 and −7/30, respectively. In case ω_{RP} is unequal to $2\omega_L$ this equation and the initial conditions give the following solution for b_{12}:

$$-\frac{1}{60}\frac{\left(2\,\omega_{RP}^2\,\omega_L^2+20\,\omega_L^4\right)\cos\left(\omega_{RP}\,t\right)}{\omega_{RP}^2\left(-\omega_{RP}^2+4\,\omega_L^2\right)} -\frac{1}{60}\frac{\left(-6\,\omega_{RP}^4+17\,\omega_{RP}^2\,\omega_L^2\right)\cos\left(2\,\omega_L\,t\right)}{\omega_{RP}^2\left(-\omega_{RP}^2+4\,\omega_L^2\right)} -\frac{1}{60}\frac{-20\,\omega_L^4+6\,\omega_{RP}^4-19\,\omega_{RP}^2\,\omega_L^2}{\omega_{RP}^2\left(-\omega_{RP}^2+4\,\omega_L^2\right)}$$

The second term has the radian frequency $2\omega_L$, which implies frequency doubling of ω_L connected to b_3 in b_1. This frequency doubling is manifest in all full solutions and was previously predicted by Longuet-Higgins[6]. The first term in the above expression has a radian frequency ω_{RP} which in normal ambient conditions is quite high (order of 10 kHz). The occurrence of this frequency necessitates a small time-step in all numerical simulations of bubble deformation with the Poisson equation.

In case ω_{RP} equals $2\omega_L$ the above differential equation for b_{12} allows for the following solution:

$$b_{12} = \{58 - 58\cos(\omega_{RP}\,t) - 7\,\omega_{RP}\,t\sin(\omega_{RP}\,t)\}/480 \qquad (38)$$

It is obvious that in this resonance case the amplitude is continuously increasing with time. In fully nonlinear simulations below it will be attempted to reach this full resonance condition.

The case $\omega_{RP} = 2\omega_L$ at ambient conditions at sea, $p_\infty = 0.1$ MPa, $\sigma = 0.07$ N/m, $\rho_L = 1000$ kg/m^3 to a bubble radius of about 7 μm. This rather small radius makes it worth the while to try to look for more cases in which b_1 exhibits resonance behavior. The third order solution b_{13} has therefore been investigated. The resulting lengthy expression for b_{31} shows asymptotic behavior for

$\omega_{RP} = \omega_L\sqrt{(5/6)}$ and for $\omega_{RP} = \omega_L\sqrt{(53/6)}$,

next to a resonance case that is close to the one found above. The situation $\omega_{RP} = \omega_L\sqrt{(53/6)}$ is at ambient conditions reached for a bubble radius of 17 μm, which is considerably higher than 7 μm. In the expression for b_{13} frequencies of oscillation occur that are not multiples of ω_L or ω_{RP}, such as $\sqrt{(\omega_{RP}^2+\omega_L/6)}$.

The above solutions have guided in the selection of process and initial conditions of full solutions, some of which have been chosen such that resonance is anticipated. The results are presented and discussed in the next section. In all non-viscous, non-resonance cases with low disturbance amplitudes the approximate solutions derived above turned out to be close to the full solutions of the Euler-Lagrange equations in the entire time domain.

Full nonlinear solutions with no wall and no damping

In order to study the characteristics of the breathing mode close to resonance it is advantageous to define λ, k and ψ, as follows, and to rewrite Eq. (34). Let

$$\lambda \equiv \varpi_3/\omega_L,\quad k \equiv \{p_L R_0/\sigma\}/\{16/\gamma - 2 + 2/(3\gamma)\},$$
$$\psi \equiv (k-1)(25-3\gamma)+24 \qquad (39)$$

In the definition of λ, frequency ϖ_3 stems from fitting and Eq. (33). With dimensionless time τ given by $t\sqrt{\{\sigma/(\rho_L R_0^3)\}}$, Eq. (34) is written as follows:

$$b_1/R_0 = 1 - 0.2\,\beta^2\{1+7\lambda^2/(\psi-24\lambda^2)\}\sin(\tau\{\sqrt{(\psi/2)} - \lambda\sqrt{12}\})\sin(\tau\{\sqrt{(\psi/2)}+\lambda\sqrt{12}\}) + -0.1\beta^2\{1+3\lambda^2/\psi+2/\psi\}\{\cos(\tau\sqrt{(2\psi)})-1\} \qquad (40)$$

The amplitude of the double sinus-term in Eq. (40) clearly increases for ψ approaching 24, which is equivalent to k approaching 1. Full resonance occurs for k equal to $\{1-24(1-\lambda^2)/(25-3\gamma)\}$, in which case the double sine term in (40) changes into a term that increases linearly with dimensionless time τ. The predictive capacity of Eq. (40) for a time comprising a multitude of cycles with duration $2\pi/\omega_L$ is investigated in Fig. 2.

Figure 2 shows that the amplitude of the double sinus-prediction of Eq. (40) is in very good agreement with the full nonlinear solution. The main radian oscillation frequency of b_3, the fitted ϖ_3 from (33), is found to be changing continuously with time. If the period of oscillation is made dimensionless with $\sqrt{\{\sigma/(\rho_L R_0^3)\}}$, as in the definition of t, the dimensionless radian frequency is at early times about 3.4135, which is less than the dimensionless frequency of ω_L, $\sqrt{12} \approx 3.4641$. At later times the radian frequency decreases even more.

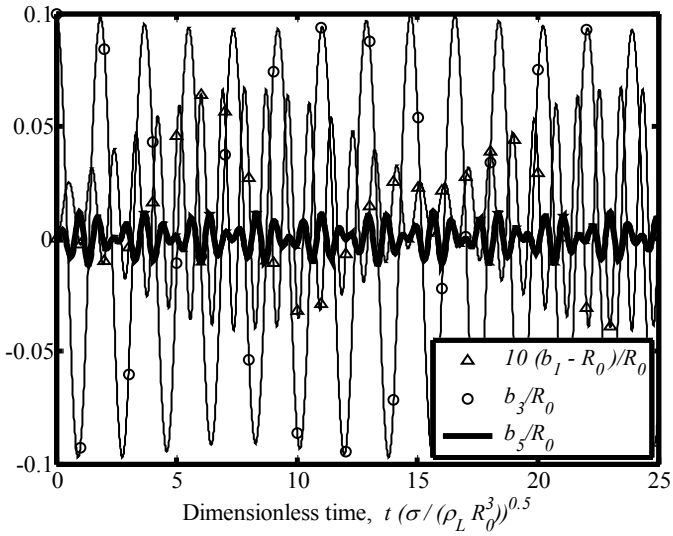

Figure 2 Shape coefficient histories for b_3-excitation with $\beta = 0.1$, $\gamma = 1.4$ and $p_L R_0/\sigma = 10.89$, *i.e.* $k = 1.1$. This condition is for example obtained with water with $\sigma = 0.07$ N/m and $\rho_L = 1000$ kg/m^3 at a pressure of 762.3 Pa, if $R_0 = 1$ mm. Values of $|b_5/b_1|$ are about 0.01 at maximum; values of $(b_1-1)/R_0$ vary between about –0.04 and 0.07.

The even coefficients b_2, b_4, …, are zero for reasons of symmetry. The first nonzero coefficient, b_5/R_0, has no contribution to $b_{1,2}$ and $b_{3,1}$ and consequently no influence on the time history of b_1 in Fig. 2. In each b_3-cycle of duration of about $2\pi/\omega_L$ where the maximum amplitude of b_1 reaches its maximum (at dimensionless times 8 and 23 in Fig. 2, for example), the

maximum amplitude of b_3 is somewhat lower than in other such b_3-cycles. Part of the surface energy of the driving mode, b_3, is apparently converted into sound-generating isotropic vibrations of the bubble, the breathing mode of b_1. As compared to cases when k is far from 1, the amplitudes this breathing mode attains are quite high. The conditions of Fig. 2, for k =1.1, are beneficial for sustained generation of sound at a reasonable level at the two frequencies of the sine-terms in Eq. (15). This condition can be obtained for R_0 = 1 mm, as in Fig. 2, but also for other pressures and surface tension coefficients as long as $p_L R_0/\sigma$ = 10.89 equals 1.1.

The closer to resonance, the higher the amplitude of b_1 gets, see Fig. 3. The corresponding shapes of the bubble are all in the range from spherical to slightly ellipsoidal, still.

The higher the maximum amplitude of b_1 during a period of dimensionless time $\pi/\{\sqrt{(\psi/2)} - \lambda\sqrt{12}\}$, about twice the time-span shown in Fig. 3, the lower the corresponding maximum of b_3, as is clearly observed in Fig. 3. In this case of k = 1, the main radian frequency of b_3 (ϖ_3 from Eq. 33) hardly varies in time since it is close to $\omega_{RP}/2$.

Although the amplitude of b_1 has been blown up considerably by selecting k = 1, and that of b_3 decreased considerably, the periodicity on the time scale $\pi/\{\sqrt{(\psi/2)} - \lambda\sqrt{12}\}$ is not lost for the above cases with initial shape deformation given by β = 0.1. Shapes remain not far from spherical, and for example b_5 is unimportant for the b_1-history. All this is not true anymore for β = 0.4, see Fig.'s 4 and 5. The shape changes considerably in this case of k = 12, σ = 0.05 N/m, ρ_L = 1000 kg/m^3, R_0 = 1 mm, γ = 0.1, $p_L R_0 / \sigma$ = 2000 (resonance value close to 164.7). Other conditions for β = 0.4 resulted in even stronger deformations. Not only the value of b_5 becomes significant, see Fig. 5, also the amplitude of b_1 is not well predicted by Eq. (40) anymore. The radian frequency ϖ_3, fitted with Eq. (33), differs by as much as 18 % of ω_L already in the first b_3-cycle.

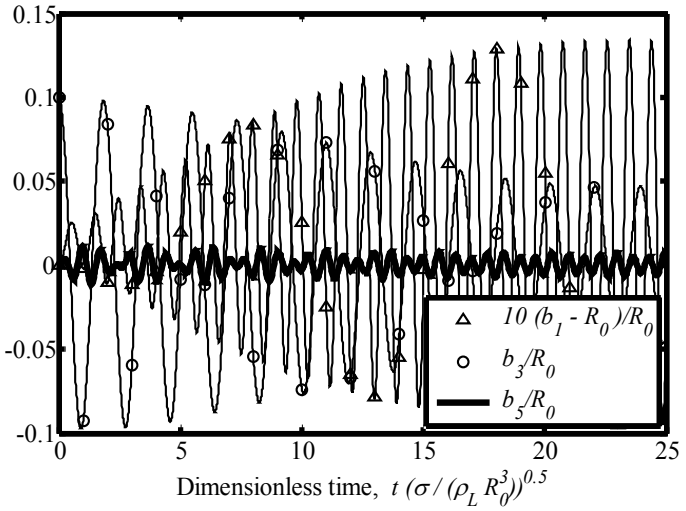

Figure 3 Shape coefficient histories for b_3-excitation with β = 0.1, γ = 1.4 and $p_L R_0/\sigma$ = 9.9048, *i.e.* k = 1.0.

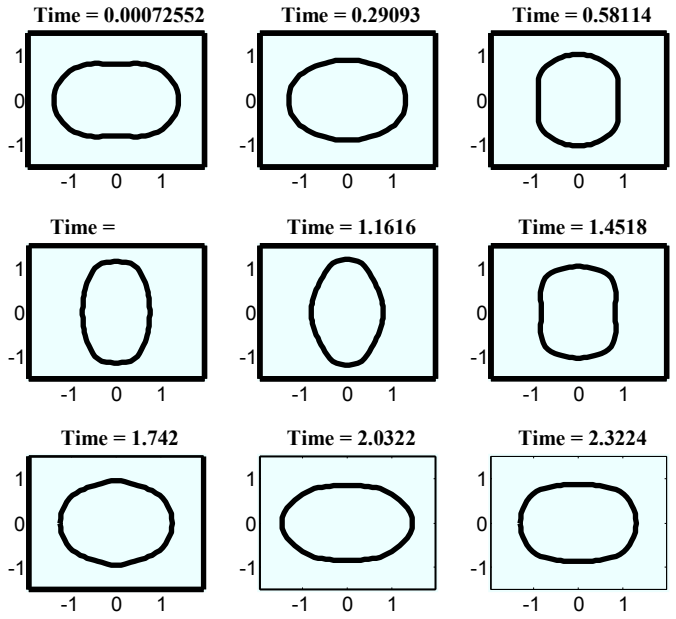

Figure 4 Shapes at various characteristic times, for b_3-excitation with β = 0.1, γ = 0.1 and $p_L R_0/\sigma$ = 2000, *i.e.* k = 12. See Fig. 5 for corresponding histories of deformation coefficients at corresponding dimensionless times.

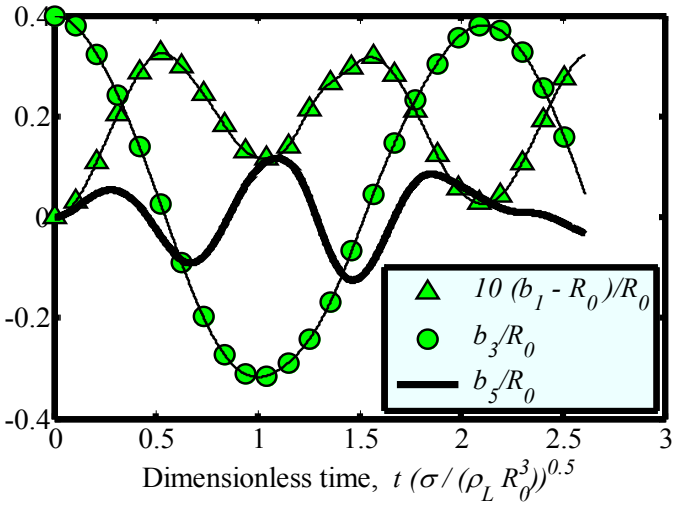

Figure 5 Shape coefficient histories for b_3-excitation with β = 0.4, γ = 0.1 and $p_L R_0/\sigma$ = 2000, *i.e.* k = 12. See Fig. 4 for corresponding shapes.

Full nonlinear solutions with nonzero viscosity

The following three dimensionless numbers have been used to specify and control the process of bubble dynamics:

$$We = U_0^2 \rho_L R_0 / \sigma,\ Psl = p_\infty / (\rho_L U_0^2),\ Re = U_0 R_0 \rho_L / \mu_L.$$

Note that the radius, not the diameter, is used in this Reynolds number. Typical velocity U_0 is arbitrary and taken to be 1 mm/s. This merely defines a unit of time as R_0/U_0. Another choice could have been based on the typical radian frequency of bubble oscillation with unit of time, τ_{osc}, equal to

$\sqrt{(\rho_L R_0^3 / \sigma)}$. Let F be defined as ω_L^2/ω_{RP}^2. The product $Psl\ We$ is given by $\{12/F - 2(3\gamma - 1)\} / (3\gamma)$ and is fixed in cases of resonance, as for example the case $\omega_{RP} = \omega_L \sqrt{(53/6)}$ found by the perturbation analysis of the previous section. The value of F specifies the resonance case. Weber number $We = 20$ and resonance case $F = ¼$ correspond to a value of Psl which is used to obtain the results of Fig. 6. An approximation of this value (0.495238095238095

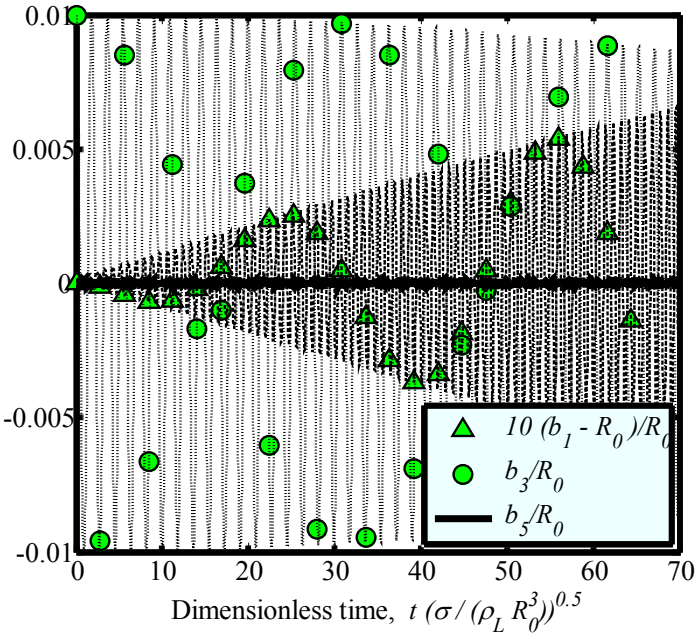

Figure 6 Shape coefficient histories for b_3-excitation with $\beta = 0.01$, $\gamma = 1.4$, Psl = 0.495238095238095, We = 20, Re = ∞ and F = 1/4. A limited number of plotting points is used.

) is given in the caption of this figure.

In agreement with the choice $F = ¼$, the initial increase of b_1 in Fig. 6 for $\beta = 0.01$ is as predicted by the resonance prediction, Eq. (38). It levels off at times exceeding 130 τ_{osc}. This leveling off is seen in Fig. 7 which is for the same conditions except for a higher initial amplitude, $\beta = 0.1$. Each time b_1 reaches its maximum value the mean value of b_3 over a period of $5\tau_{osc}$ is lowest. Energy in the isotropic mode is gained at the expense of energy in the anisotropic mode. Note that the value of b_5 is negligible at all times.

For F =1, so close to the value (5/6) found via b_{31} under (38), the amplitude of b_1 is found to increase, be it at a smaller rate than in previous figures since this resonance case corresponds to b_{13} so is proportional to β^3. In this near-resonance case b_3 has an almost equal period of oscillation as b_1, in agreement with the choice $F = 1$.

Viscous solutions show damping, as is shown in Fig. 8 for $F = 0.2575$ and $Re = 1000$. The initial distortion and the initial excess in pressure, see the discussion under Eq. (17), are converted into a mean expansion, as reflected by the nonzero positive value of the b_1-value averaged over times exceeding $100\tau_{osc}$, and into an oscillation of b_1. This oscillation pertains over far longer times than during which the anisotropic deformation is discernable. Longer time histories have been computed but are not plotted for sake of clarity of the figures.

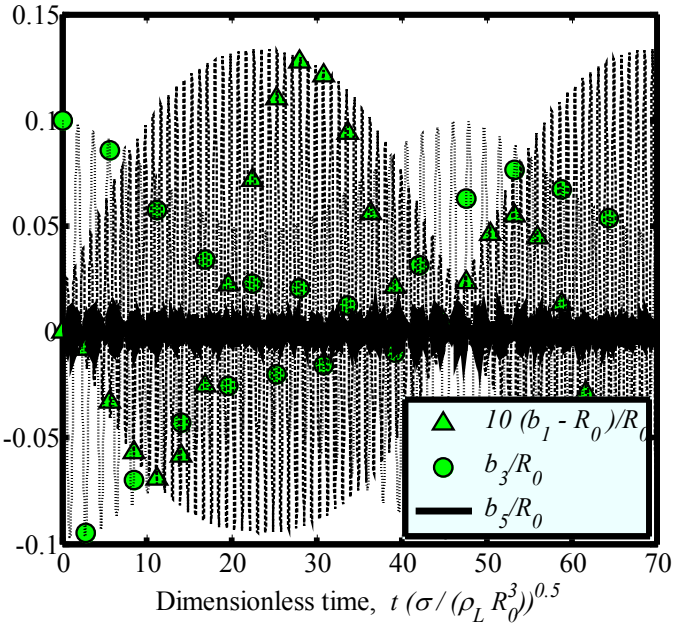

Figure 7 Shape coefficient histories for b_3-excitation with $\beta = 0.1$, $\gamma = 1.4$, Psl = 0.495238095238095, We = 20, Re = ∞ and F = 1/4. Values of $|b_5/b_1|$ are about 0.01 at maximum; values of $(b_1–1)/R_0$ vary between about –0.09 and 0.13.

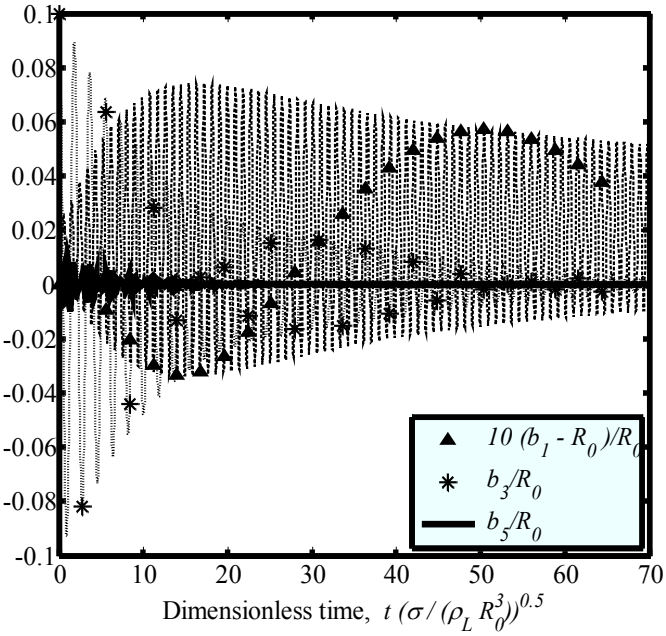

Figure 8 Shape coefficient histories for b_3-excitation with $\beta = 0.1$, $\gamma = 1.4$, $Psl = 0.4787$, $We = 20$, $Re = 1000$ and $F = 0.2575$.

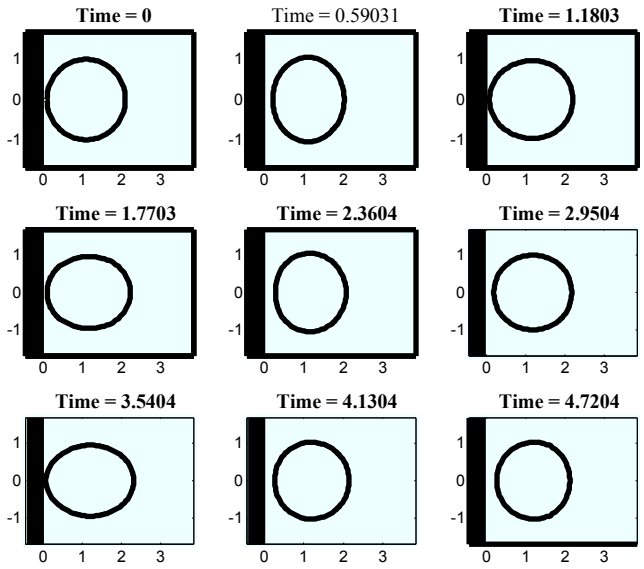

Figure 9 Bubble shape at equidistant dimensionless time instants for $We = R_0\,\rho_L\,(\mathrm{d}b_3/\mathrm{d}t|_0)^2/\sigma = 0.12$. The dimensionless times indicated are given by $t\,\sqrt{\{\sigma/(\rho_L\,R_0^3)\}}$, with R_0 the initial radius. Initial velocity, U_0, is zero, $h_0/R_0 = 1.1$ ($g_0 = 1/2.2$) and $\gamma = 1.4$.

ACOUSTIC INDUCED BUBBLE OSCILLATION AND DEFORMATION NEAR A PLANE WALL

The eigenfrequencies of bubbles were in the previous section found to depend on the initial disturbance amplitude, on the presence of a wall and on system pressure and physical properties. Because of the importance for boiling bubbles, the effect of a wall is further studied below, in particular for cases with bubble excitation by sound waves.

Full solutions without sound excitation

An initially spherical bubble has a center point at distance h from a plane wall. The velocity of its center point, U, is initially zero. Coordinate b_2 equals h in this case. The main deformation mode is described by b_3 and corresponds to elongation normal to the wall, as shown by the results of Fig. 9 for an initial velocity $\mathrm{d}b_3/\mathrm{d}t$ unequal to zero. Let $g = R_0/(2\,h)$ be the dimensionless distance to the wall halved. The governing equation for b_3 can be simplified to:

$$b_1\,\mathrm{d}^2b_3/\mathrm{d}t^2 + (2/7)\,b_1^2\,(\mathrm{d}b_3/\mathrm{d}t)^2\,(1 + 29(b_3/b_1)/14) =$$
$$-12\,\sigma\,(b_3/b_1)/(R_0\,\rho_L) - U^2/4 - U\,\mathrm{d}b_3/\mathrm{d}t\,g^2/2 \qquad (41)$$

from which the dominant frequency $\omega_L = \sqrt{\{12\,\sigma/(R_0^3\,\rho_L)\}}$ easily follows. Similarly, for mode 5 the frequency $\omega_{L,5} = \sqrt{\{90\,\sigma/(R_0^3\,\rho_L)\}}$ is derived; for higher modes the frequencies are higher still. Closer to the wall, the deformation induces a non-zero velocity U that also affects the main radian frequency. For the breathing mode, for example, the main frequency, ω, is found to be given by

$$\omega^2 = \omega_{RP}^2\,/\,\{1 + g_0 - 3\,g_0^4/(4\,\alpha)\} \qquad (42)$$

with the added mass coefficient α about 0.7 and g_0 the initial dimensionless distance defined above. The substantial frequency decrease given by this equation is well confirmed by fully nonlinear computations. Close to the wall, ω is given by

$$\omega = \omega_{RP}/1.2 = 2\,\pi/T_{RP}/1.2 \qquad (43)$$

Various fundamental mode oscillations close to the wall have been studied. For $\beta = 0.1$ and $g_0 = 1/2.2$ the radian frequency is typically found to be 10 % less than that of a free bubble with the same initial deformation. For this reason it is to be anticipated that a bubble attached to a plane wall and that is made to execute an oscillatory deformation motion with main component b_3 has a main frequency well below ω_3. This will be experimentally investigated below.

When selecting a sound wave to excite isotropic bubble deformation, the breathing mode, Eq. (43) gives guidance. But close to the wall dispersion takes place, *i.e.* also other normal deformation modes are activated as well. This is further investigated below.

Full solutions with sound excitation

At acoustic frequencies of about 3 kHz, pressure oscillations induced by sound are spatially homogeneous on the scale of the bubble, since bubble radius is of the order of 1 mm while the acoustic wavelength is of the order of 1 m. The acoustic wave is therefore modeled as an oscillating contribution to the system pressure in the liquid. Since the value of γ is 1.337 for water vapor at 100 °C and 0.1 MPa, this value will be used in the computations below. The value of γ has been varied between 1.0 and 1.4 with hardly an effect on the shape amplitudes found. The higher γ, the better volume is conserved and the smaller the amplitude of isotropic deformation (the breathing mode corresponding to b_1) computed for a given sound wave. Previous experiments at system pressure 10^5 Pa yielded boiling bubbles with a volume-equivalent radius in the range 0.9 to 1.0 mm during 70 % of its lifetime before detachment from the wall, *i.e.* during 6 ms. Because of the dependency of oscillation frequency on initial disturbance amplitude, a sound wave with small amplitude, 20 Pa, will be assumed to occur at the location where bubbles are created. Computations will now be shown with the two representative values 0.9 and 1.0 mm of the bubble radius. In these computations, the excitation of the sound wave is given by

$$p_{\infty,a} = 20\,\sin(2\,\pi\,t/T_{RP}) \qquad (44a)$$

or by

$$p_{\infty,a} = 20\,\sin(2\,\pi\,t/T_{RP}/1.2), \qquad (44b)$$

where the factor 1.2 accounts for the presence of the wall, see (44). The total pressure far away from the bubble is given by $p_\infty + p_{\infty,a}$.

A total number of 30 generalized coordinates have been used in the computations to warrant full convergence. To avoid redundancy, coefficient b_2 is replaced by the distance of the bubble center to a wall, h, whenever h exists.

If both R_0 and R_{00} are taken to be 1.0 mm, if (44b) is used and if the initial distance of the center of the bubble to the wall, $h(0)$, is 1.1 mm, the time histories of the coordinates shown in Fig. 10 are computed.

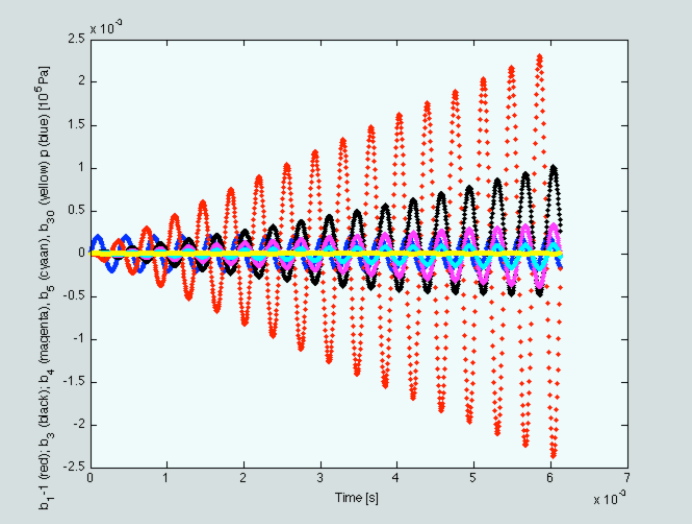

Figure 10 Time histories of various generalized coordinates, in mm, in the on-resonance case. The red curve is b_1–1, the black one is b_3, the magenta one b_4, the cyan one b_5. The yellow line represents b_{30} which is shown to remain insignificant at all times. The blue curve with constant amplitude 20 Pa is the enforced acoustic pressure wave, $p_{\infty,a}$.

The amplitude of the isotropic component, b_1, is 2.5e-3 mm at time 6 ms and increases all the time. It looks like resonance spot-on, although comparison with Fig. 6 shows that longer times should be computed to be sure. For this reason, another case will be investigated shortly. Asymmetric deformation is apparent in the nonzero, oscillating values of b_3 in the sense that positive and negative deformations differ. Full convergence is reached at all times (yellow curve of b_{30}). Note that after some time many natural modes, *i.e.* many b_j-components, are actually contributing to the deformation. The initially isotropic deformation degenerates into a more complex deformation because of non-linearity and the presence of the wall. Relative volume change is 7e-3 at final time 6 ms, see Fig. 11.

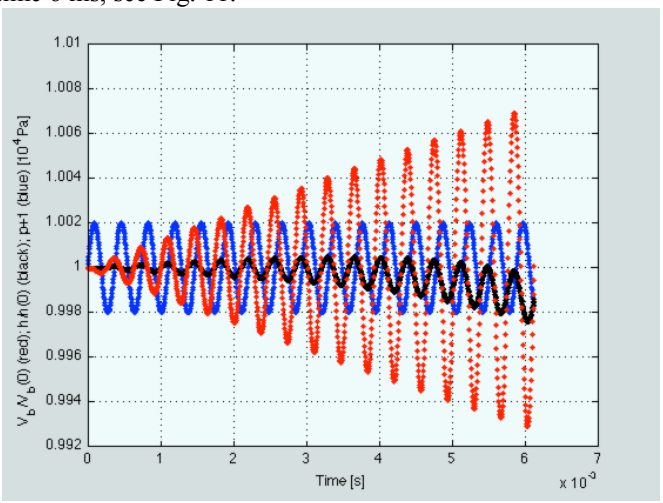

Figure 11 Time histories of relative volume change, $V_b/V_b(0)$, motion of the center of the bubble to the wall as the relative distance to the wall, $h/h(0)$, in black and of 1 + the imposed acoustic pressure $p_{\infty,a}$ (blue). This case corresponds to that of Fig. 10.

On the long run, the bubble is found to approach the wall (h-history in Fig. 11), in agreement with the Bjerkness force [21, p. 345].

For better understanding of the above results, bubble behavior with the same acoustic excitation, with T_{RP} equal to 0.36 ms, as in the above computation but with different initial radius, R_0 = 0.9 mm, is investigated now. Some typical findings are gathered in Fig. 12.

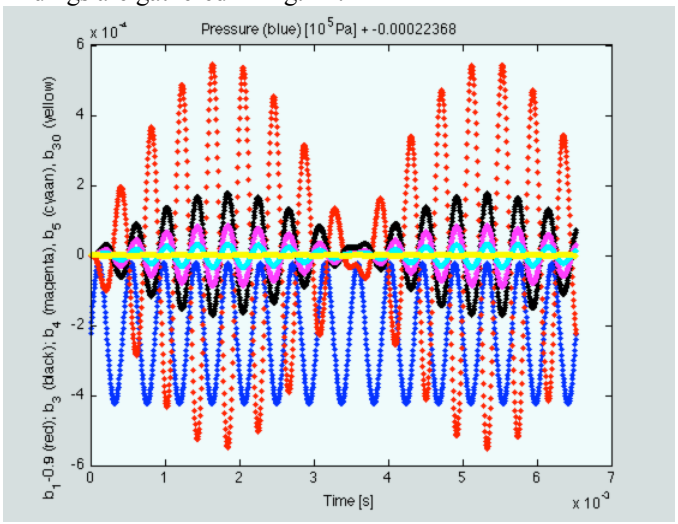

Figure 12 Time histories of various generalized coordinates, in mm, in an off-resonance case. The red curve is b_1–1, the black one is b_3, the magenta one b_4, the cyan one b_5. The yellow line represents b_{30} which is shown to remain insignificant at all times. The blue curve with constant amplitude 20 Pa is the enforced acoustic pressure wave, $p_{\infty,a}$.

The continual increase of amplitudes of Fig. 11 appears to be replaced by an oscillatory behavior with a longer time scale, of about 7 ms (Fig. 12). This time scale corresponds to the Lamb-frequency of the b_3 coordinate, $\omega_L = \omega_3$. This is a direct consequence of the fact that all natural modes are coupled via a matrix equation of the form (13). The dispersion caused by the first off-diagonals in matrix $\boldsymbol{A}$ is shown clearly in Fig.'s 10 and 12. The Euler-Lagrange equation for the anisotropic deformation component b_3 is given by Eq. (41). It exhibits a direct coupling of b_3 with b_1 and h, which explains the low frequency envelope of Fig. 3.

One important difference with actual boiling bubbles is the fixation of the bubble foot to the wall. The constraint hampers acceleration of liquid near the contact line of the three phases. This is felt as an additional force counteracting acceleration, which implies an increase in the inertial, added mass. An increase in added mass lowers the natural frequency of the breathing mode, just as the factor 1.2 in (43) and (44b) in the above section does. Jiri Vejradzka[13] varied the fixation of a bubble foot attached to a solid ring and predicted natural frequencies with a linear disturbance approach. He found that with increasing angle of attachment of the bubble to the ring, so with increasing bubble contact area with the wall, the hampering of fluid acceleration becomes less and the resonance frequency increases. In the following, an experiment is described to determine the resonance conditions

actually occurring during boiling bubble growth on a plane wall.

EXPERIMENTAL VALIDATION WITH ACOUSTIC EXCITATION

Douglas *et al.*[35] applied rather strong sinusoidal acoustic waves, with amplitudes reported exceeding 1 kPa and up to 40 kPa on a single boiling bubble. Frequencies were in the range 2-23 kHz, so audible at the lower end. The main result of increasing amplitude was presented in their Fig. 6: with increasing amplitude more harmonics are induced and with even higher amplitude a broadband spectrum with the driving frequency as the only distinct one is excited. The lower the amplitude, the better the acoustic energy is targeted at a selected frequency. At the same time: the lower the amplitude, the better the predictive capacity of natural frequencies of disturbance analysis is, as demonstrated amply in the above. For these reasons, experiments have recently been performed with acoustic waves with low amplitude exciting a boiling bubble.

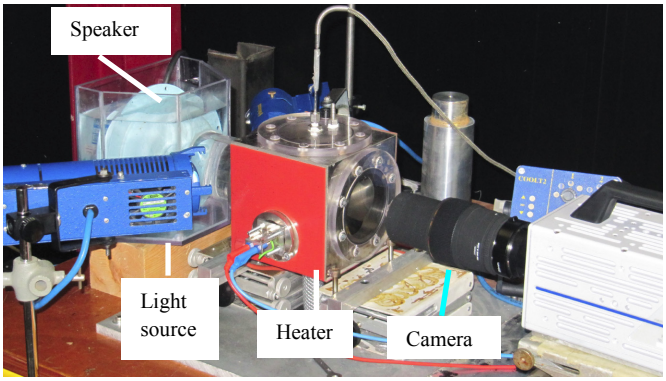

Figure 13. Photograph of the total set-up. The red heating pad has the bubble generator passing through.

Boiling set-up and bubble generator

The main part of the experimental setup consisted of a pool boiling vessel. Heating elements heated up both the fluid and the vessel, to minimize heat losses from the fluid to the surroundings during the actual experiments. The fluid was deaerated, deionized water at near-saturation temperature and at ambient pressure. Figure 13 shows an overview of the experimental setup. More details are given in [30].

A so-called bubble generator is positioned in the center of a cross-section of the vessel that is at about 2 cm from the bottom. It is used to locally heat up the bulk fluid and generate boiling bubbles. It has a thin sheet of stainless steel on top of its surface, embedded in non-conducting and temperature resistant glue, see Fig. 15. Joule's heat heats up the ambient of a circular hole with a diameter of 30 μm that leads to an artificial air pocket underneath the thin sheet. In this way a single active nucleation site has been activated. The bubbles had nearly constant detachment volume and growth time if nothing else was changed in the process conditions.

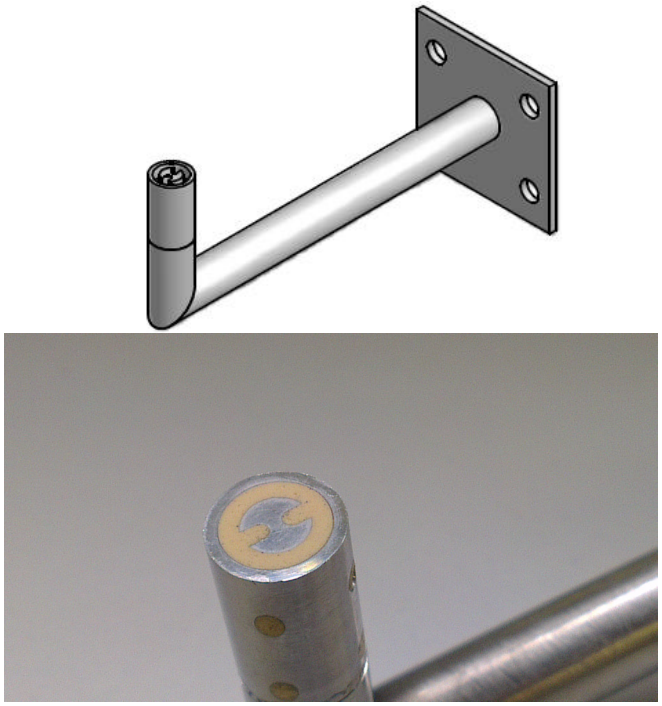

Figure 14 Schematic drawing and photograph of the bubble generator. Constant direct current heats up about 1 mm^2 around a small hole which is the exit of an air-filled cavity at the back of a stainless steel strip which is welded on two solid rounded bars.

A reservoir containing a sonic speaker was connected to the pool boiling vessel, with a white polymer membrane in between, clamped to one side of the boiling vessel. A Photron Fastcam SA3 operated at a frame rate of 3000 fps (frames per second) and a resolution of 512 x 256 $pixels^2$ made recordings of approximately 7 s each. Each recording shows undisturbed boiling bubbles during about 3.5 s before and acoustically excited boiling bubbles during the subsequent 3.5 s. The relative error of the volume equivalent radius determined from the recordings, R_{eq}, is about 0.7 % in the final stage of bubble growth.

The sonic speaker was excited by continuous sinusoids of varying frequency. The sound pressures applied to the boiling bubbles at the location of the bubble generator were measured by replacing the bubble generator with a hydrophone (8103, Bruel & Kjaer, Naerum, Denmark). The pressure at the bubble generator varied between 15 and 22 Pa for the applied frequency range 3 – 5 kHz.

Some experimental results

There is a high reproducibility of the bubble size history prior to excitation with sound. The error in each individual measurement of the equivalent diameter is estimated at about 0.014 mm, but the reproducibility in the final stage of bubble growth is much better. With sound, the final 6 s of bubble growth are different in that the bubble diameter is smaller and the bubble growth rate is somewhat less. When the final equivalent radius of each bubble is determined and is used to compute the equivalent volume, $4\pi R_{eq}^{\ 3}/3$, no change in this volume is detected as long as the sound is not switched on.

At the acoustic frequencies applied, pressure oscillations induced by sound are spatially homogeneous on the scale of the bubble, as discussed earlier. Oscillation time corresponding to these acoustic waves is about 0.33 ms, which implies that the number of pressure oscillations felt by a bubble during its growth is typically 30. The nonlinear computations of bubble deformation in the vicinity of a plane wall of the previous section permit the following estimations of actual bubble deformation during growth. At resonance, the relative isotropic radial displacement can be about 2.5 μm in a time span of 6 ms. Deformations of this size cannot be observed with the spatial resolution of the lens system used. Despite of this, the bubble size at detachment was found to decrease near resonance.

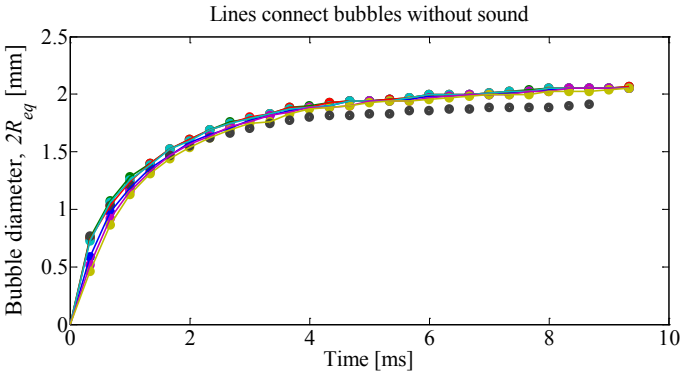

Figure 15 Histories of bubble diameter for various bubbles without and one bubble measured with acoustic excitation. The excited bubble detaches 0.7 ms faster with a diameter which is 7 % less.

Figure 15 shows how detachment is affected by acoustic excitation when the frequency of sound is properly selected. During each measurement, acoustic excitation occurs after a couple of seconds. Let $R_{eq}(0)$ be the equivalent radius at detachment of the first bubble during the same recording, without acoustic excitation, and R_{eq} the equivalent radius of the last bubble, with acoustic excitation, during a single measurement. In [30], values of the maximum difference in relative equivalent volume, $\{(R_{eq}/R_{eq}(0))^3 - 1\}$, are studied. The acoustic frequency applied is subtracted of the frequency ω_{RP} predicted with Eq. (16) and divided by 1.2 to account for the wall. The resulting difference is zero at the predicted resonance frequency. A plot of $\{(R_{eq}/R_{eq}(0))^3 - 1\}$ versus the difference in predicted and applied frequencies is found to have a distinct peak at the value zero [30]. These findings appear to be a confirmation of the predictive capacity of (16) and the correction factor 1.2. The paper [30] argues why the agreement found is due to different physical agencies that are compensating one another.

Whatever the nature of the compensating agencies, resonance of isotropic deformation, the breathing mode, of a bubble attached to a plane wall is well predicted from the Rayleigh-Plesset frequency given by (16), divided by 1.2, if for the radius the detachment radius without sound is used.

EXPERIMENTAL VALIDATION WITHOUT ACOUSTIC EXCITATION

Douglas *et al*[35] observed capillary waves and diameter oscillations on the bubbles, as well as destruction of bubbles, the occurrence of both Bjerkness forces. With increasing frequency the knockoff bubble diameter decreased from about 2 to 0.4 mm. The optimal frequency, f, for removal of a vapor bubble was presented to be given by $f^2 \approx 300\ \sigma / (D^3 \rho_L)$, be it with only 4 diameters observed below 1.1 mm. This is fairly close to the frequency of the first mode we have measured for a bubble attached to a site: $f^2 \approx 394\ \sigma / (D^3 \rho_L)$. This observation is one of the reasons why their optimal frequency is believed to be related to ω_L-frequencies of anisotropic shape oscillations and not to the resonance frequency of the breathing mode, ω_{RP} as predicted by (16). The dedicated experiments that produced $f^2 \approx 394\ \sigma / (D^3 \rho_L)$ are described below.

Boiling set-up and bubble generator

Demineralized and degassed water is pumped through a closed tubing system of stainless steel piping with an inner diameter of 38.7 mm. A reservoir on top of the test rig contains a stratified pool of liquid with a moist air mixture on top that can be vented to the ambient. Slightly subcooled water flows from this reservoir to the vertical test section via a preheater, a firerod submersion heater. At the measuring location, absolute pressure is around 1.3 bar and liquid temperature, T_L, is at saturation or very close. Upstream of the measuring section a flow straightener is used to minimize swirling and secondary motion in the downward pipe flow. In the center of a transparent piece of test section (quartz) with the same inner cross-section as the other tubing a bubble generator is located, see Fig. 14 and the description above. This generator has a flat circular top end of 10.0 mm with a hole in its center. The diameter of this hole, a cavity mouth, is 40 μm in this case. An area of around 1 mm^2 around the mouth is heated with Joule's heating of a thin (150 μm) metal strip that constitutes part of the top of the bubble generator.

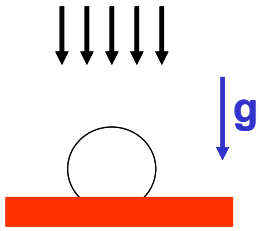

Figure 16 Schematic of stagnation flow onto the bubble generator with artificial cavity.

The velocity field that approaches the bubble generator in downflow has been measured with LDA. The mean mass flow rate is continuously measured with a Coriolis-meter. Reynolds number has been in the range 5600 – 22400 corresponding to mean velocities of 4.3 to 17.0 cm/s at 100 °C. Static pressure and temperature at the measuring location are measured with accuracies of 1 % and 0.1 °C, respectively. Because of the downflow, a stagnation flow is created on top of the bubble generator, see Fig. 16.

The quartz test section is equipped with four flat surfaces, facets, to minimize optical distortion. The same high-speed video camera (PCO 1200 hs) has been used, as well as a microscope lens and diffuse background illumination with a 250 W cooled halogen lamp have been used to observe growth and detachment at a frame rate of 3500 Hz and a resolution of 220 x 200 pixels^2. Typically, a resolution of 10 μm per pixel was applied. Distances have been calibrated with the aid of a small plate with 10 holes (1.0 mm diameter) positioned at known location above the bubble generator. Image processing with subpixel-accuracy is used to analyze recordings. Stereoscopic recordings proved the bubbles generated to be axisymmetric and fully stable in azimuthal direction. Both flow to the bubble generator and shape deformation is fully axisymmetric at all times. Subsequent recording have therefore been side-views only.

All experiments reported below were performed with the same condition of water during one day, with the same nucleation site activated. Reproducibility of bubble growth and detachment is therefore high. The main process conditions varied are:

- The mean velocity of the approaching flow, v_L.
- The bulk temperature of the approaching flow, T_L, or equivalently its sub-cooling $T_L - T_{sat}$ with T_{sat} the saturation temperature of the local system pressure, 0.13 MPa.
- The power to the bubble generator, P, or the super-heating of the wall, $T_w - T_{sat}$.

The average number of bubbles analyzed for each of the conditions applied is 30. The time of attachment has typically been in the range 60 – 180 ms. At the highest v_L, the liquid sub-cooling has been 3.5 ± 0.75 K, with standard deviation σ_T = 0.75 K measured over a period of 2 seconds.

Some experimental results

Figure 17 shows typical histories of the main length scales of the bubble attached to a plane wall. The inserts are pictures of the bubble shape at the times indicated with black dots. Axisymmetric elongation in the direction away from the wall is observed. The frequency of oscillation is strongly dependent on time, as is either one of the lengths scales. All bubbles exhibited a similar continued shape oscillation.

A frequency analysis of the shape oscillation has been performed in the following way. The total growth time is divided into time periods, named windows, of the order of about 2.8 oscillation cycles. The window changes size in the course of time. Fourier analysis with Hanning windowing and zero's padding to increase accuracy is applied to each individual window. The program has been validated with constructed test cases with known input frequencies and random numbers.

The period of oscillation, T, during many experiments is found to correlate very well with R, defined as the radius of curvature at the top of the bubble, *i.e.* the point at the vapor-liquid interface furthest away from the wall, the top of the bubble generator. The parameters C and m in the following defining equation (44)

$$T = \mathrm{C}\, R^m \sqrt{(\rho_L/\sigma)} \qquad (44)$$

have been determined by fitting to data of more than 100 bubbles. For each operating condition, the same values of C and m have been found. The value of m is 1.49 ± 0.02. Note from the above sections that each period of oscillation of a free bubble deforming in a fundamental mode is proportional to $R^{3/2}\sqrt{(\rho_L/\sigma)}$. The value of m found has been determined in this dedicated experiment with high accuracy, because of the long time the bubble resides in the downward stagnation flow. The value of m found is 3/2 and with certainty points out that the oscillation deformation is related to ω_L rather than ω_{RP} since the dominant term in ω_{RP} is the pressure related first term which gives a proportionality of ω to R.

For attached boiling bubbles C is found to amount 1.9√12, an increase by 90 % with respect to the third fundamental mode of a free bubble, $\omega_L = \omega_3$. The difference is *not* explained by the measurement accuracy, also *not* those related to the continuous growth of the bubble. The difference by 90 % is *not* explained by a difference in definition (R is here the radius of curvature of the top, not the volume-equivalent radius). The decrease in frequency by 90 % is also *not* really explained by the proximity of the wall, since the resulting decrease has been found to be about 10 % in one of the above sections. The decrease by 90 % is only partly explained by finite amplitude oscillation, which has been shown to decrease the frequency in one of the sections above. The proper explanation for the experimental finding is the attachment of the bubble to the wall[34]. Simulations with the Euler-Lagrange approach described above require the extension with a Lagrangian multiplier to account for the attachment to the wall. This is work in progress.

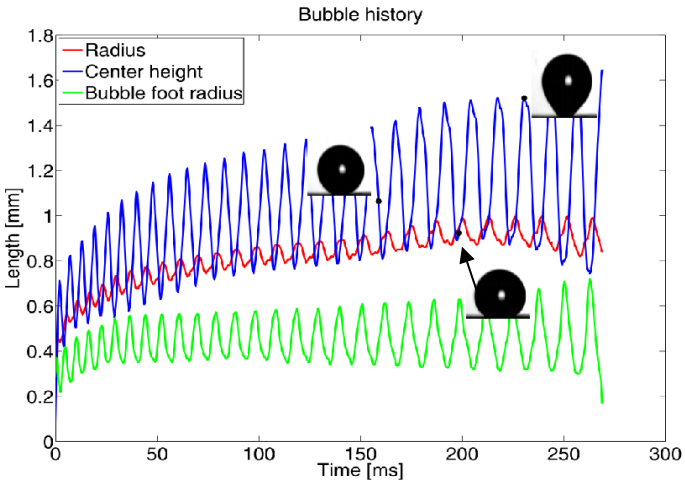

Figure 17 Histories of three main lengths of a boiling bubble in downward stagnation flow. Typical bubble shapes (inserts) at times indicated by black dots in the figure.

CONCLUSIONS

The Euler-Lagrange approach has been used to examine various aspects of boiling bubble deformation and oscillation.

- Conversion of arbitrary large-amplitude bubble deformation into isotropic deformation is found to occur naturally and is easily explained by the strong coupling of the first row, representing isotropic

deformation, of the added mass matrix $\boldsymbol{A}$ with other normal modes.

- Resonance cases in which this conversion is amplified or in which several different bubble sizes at a time are excited have been predicted with the aid of a nonlinear perturbation analysis.
- The effects of finite amplitude oscillation and the proximity of the wall on oscillation frequency have been quantified.

Isotropic boiling bubble oscillations have been excited by single frequency acoustic waves. The excitation has been found to confirm predictions of frequency reduction by the presence of the wall. Anisotropic boiling bubble oscillations have been excited in a downward stagnation flow when the bubble is created on an artificial cavity. The fundamental frequency involved has been determined experimentally and is identified as an anisotropic oscillation mode for which the constraint of bubble foot attachment to the wall is essential.

Acknowledgments

The author is grateful for the contributions of and fruitful discussions with several people, amongst whom Paul van Neer, Coen Baltis and Hans Kuerten in particular. Experimental contributions of MSc students Bram van de Sande and Remco van de Berg are gratefully acknowledged. Boiling research at Eindhoven University of Technology is currently supported by the Dutch Technology Foundation STW, applied science division of NWO and the Technology program of the Ministry of Economic Affairs. This study is part of COST action MP1106, Smart & Green Interfaces.

REFERENCES

[1] Lamb H., *Hydrodynamics,* 6th edition., Cambridge University Press, 1932, p. 117 & p. 475

[2] Longuet-Higgins, M.S., "Monopole emission of sound by asymmetric bubble oscillations. Part 1, normal modes", J. Fluid Mechanics, Vol. 201, 1989, pp 525-541

[3] Prosperetti A., "Linear oscillations of constrained drops, bubbles, and plane liquid surfaces", Phys. of Fluids, **24**, 2012, 032109

[4] Lu H.L.& Apfel R.E., "Shape oscillations of drops in the presence of surfactants", J. of Fluid Mech. **222**, 1991, pp. 351-368

[5] Miller C.A. & Scriven L.E., "Oscillations of a fluid droplet immersed in another fluid", J. of Fluid Mech. **32**, 1968, pp. 417-435

[6] Longuet-Higgins M.S., "Monopole emission of sound by asymmetric bubble oscillations. Part 2. An initial value problem", J. Fluid Mech. **201**, 1989, pp. 543–565

[7] Prosperetti A., Crum L., Commander K., "Nonlinear bubble dynamics", J. Acoust. Soc. Am. **83** (2), 2002, pp. 502-514

[8] Hegedüs F., Hös C., Kullmann L., "Influence of heat transfer on the dynamic response of a spherical gas/vapour bubble", Int. J. of Heat and Fluids Flow, **31**, 2010, pp. 1040-1049

[9] Kamath V., Oğuz H., Prosperetti A., "Bubble oscillations in the nearly adiabatic limit", J. Acoust. Soc. Am. **92** (4), 1992, pp. 2016-2023

[10] Chebel N.A., Risso F., Masbernat O., "Inertial modes of a periodically forced buoyant drop attached to a capillary", Physics of Fluids **23** (10), 2011, 102104

[11] Tsamopoulos, J.A. & Brown, R.A., "Nonlinear oscillations of inviscid drops and bubbles", J. Fluid Mechanics, Vol. 127, 1983, pp. 519-537

[12] Bostwick J.B. & Steen P.H., "Coupled oscillations of deformable spherical-cap droplets. Part 2. Viscous motions", J. Fluid Mech. **714**, 2013, pp. 336-360

[13] Vejrazka, J., Vobecka, L. and Tihon, J., "Linear oscillations of a supported bubble or drop", Physics of Fluids **25**, 2013, 062102

[14] Chesters A., "Modes of bubble growth in the slow-formation regime of nucleate pool boiling", Int. J. Multiphase Flow **4**, 1978, pp. 279-302

[15] Brenner M.P., Hilgenfeldt S., Lohse D., Single-bubble sonoluminescence, Rev. of Moderen Physics, Vol. 74, 2002, pp. 425-484.

[16] Nigmatulin I., *Dynamics of Multiphase Media*, Vol. 1, Hemisphere, Washington, 1991

[17] Prosperetti, A., "Bubble-related ambient noise in the ocean", J. Acoust. Soc. Am., Vol. 84 (3), 1988, pp. 1042-1054

[18] Prosperetti, A. and Lu, N.Q., "Cavitation and bubble bursting as sources of oceanic ambient noise". J. Acoust. Soc. Am., Vol. 84 (3), 1988, pp. 1037-1041

[19] Lighthill, M.J. "On sound generated aerodynamically. I. General theory", Proc. R. Soc. London Ser. A, Vol. 211, 1952, pp. 564-587

[20] Plesset, M.S. & Prosperetti, A. "Bubble dynamics and cavitation", Ann. Rev. Fluid Mech., Vol. 9, 1977, pp. 145-185

[21] Leighton, T.G., *The acoustic bubble*, Academic Press, London, 1994

[22] Minnaert, M., "On musical air bubbles and the sounds of running water". Phil. Mag., Vol. 16, 1933, pp. 235-248

[23] Hao Y. & Prosperetti A., "The dynamics of vapor bubbles in acoustic pressure fields", Phys. of Fluids, **11**, 2008, pp. 1999-2019

[24] Gumerov N., "Weakly non-linear oscillations of the radius of a vapour bubble in an acoustic field", J. Appl. Math. Mech., PMM USSR, **55**, 1991, pp. 205-211

[25] Gumerov N., "Dynamics of vapor bubbles with nonequilibrium phase transitions in isotropic acoustic fields", Phys. of Fluids, **12**, 2000, pp. 71-88

[26] Patel G., Nicholas R., Finch R., "Rectified heat transfer in vapor bubbles", J. Acoust. Soc. Am. **78** (6), 1985, pp. 2122-2131

[27] Hao Y. & Prosperetti A., "Rectified heat transfer into translating and pulsating vapor bubbles", J. Acoust. Soc. Am. **112** (5), 2002, pp. 1787-1796

[28] Shpak O., Kokhuis T. and Luan Y., Lohse D., Jong N. de, Fowlkes B. and Fabiili M., Versluis M., "Ultrafast dynamics of the acoustic vaporization of phase-change microdroplets", J. Acoust. Soc. Am. **134** (2), 2013, pp. 1610-1621

[29] Douglas Z., Boziuk T., Smith M., Glezer A., "Acoustically enhanced boiling heat transfer", Phys. of Fluids, **24**, 2012, 052105

[30] Geld C.W.M. van der, Neer P. van, Sande B. van de, Lexmond A., "Low-amplitude acoustic enhancement of bubble detachment in pool boiling", Phys. of Fluids, to be submitted, 2014

[31] Geld C.W.M. van der, Colin C., Segers Q.I.E., Pereira da Rosa V.H. & Yoshikawa H.N., "Forces on a boiling bubble in a developing boundary layer, in microgravity with g-jitter and in terrestrial conditions", Physics of Fluids, **24** (8), 2012, 082104

[32] Geld C.W.M. van der, "The dynamics of a boiling bubble before and after detachment", Heat Mass Transfer, **45**(1), 2009, pp. 831-846

[33] Geld C.W.M. van der & Kuerten J.G.M., "Axisymmetric dynamics of a bubble near a plane wall", J. Fluid Mech., **640**, 2009, pp. 267-305

[34] Geld C.W.M. van der, "On the motion of a spherical bubble deforming near a plane wall", J. Eng. Math., **42**(1), 2002, pp. 91-118